Chemical Geology 667 (2024) 122333

Contents lists available at ScienceDirect

Chemical Geology

journal homepage: www.elsevier.com/locate/chemgeo

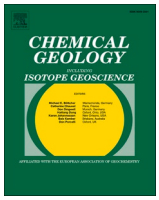

# Exploring intrusive processes through the crystal cargo of volcanic rocks: The case of lava flows from Taranaki volcano, New Zealand

Nessa G. D'Mello [a], Georg F. Zellmer [b,*], Teresa Ubide [c], John Caulfield [d], Masako Usuki [e], Yoshiyuki Iizuka [e], Gabor Kereszturi [b], Jon N. Procter [b], Robert B. Stewart [b]

[a] Department of Earth Sciences, Southern Methodist University, Dallas, TX 75205, USA
[b] Volcanic Risk Solutions, Massey University, Palmerston North 4410, New Zealand
[c] School of the Environment, University of Queensland, St Lucia 4072, Queensland, Australia
[d] Central Analytical Research Facility, Queensland University of Technology, Brisbane 4000, Queensland, Australia
[e] Institute of Earth Sciences, Academia Sinica, Taipei 11529, Taiwan, ROC

ARTICLE INFO

Editor: Claudia Romano

*Keywords:*
Plutonic basement
Mush pockets
Antecrysts
Xenocrysts
Remobilisation

ABSTRACT

The present-day edifice of Taranaki volcano, New Zealand, is largely made up of lava flows extruded over approximately the last 8 kyr. The crystal cargo of plagioclase, pyroxene and amphibole in these lavas displays varied major, minor, and trace element zoning patterns, pointing to long and complex crystal growth histories. Crystal zoning patterns do not vary systematically between stratigraphic units, and multiple patterns are seen within the same sample over very short length scales. Intracrystalline elemental variations reveal mineral-melt interactions, which result in repeated resorption and recrystallisation in varied environments. Variable degrees of undercooling are evidenced by clinopyroxenes, with most crystals displaying sector zoning ($\Delta T < 50$ K), while others only show concentric zoning, which suggests very low $\Delta T$. The common occurrence of resorbed cores within the crystals and the prevalence of glomerocrysts indicate antecrystic and/or xenocrystic origins and crystal aggregation processes. We hypothesise that the repeated intrusion of melts into the crustal basement of Taranaki volcano has resulted in the formation of a heterogeneous subsolidus plutonic to supersolidus mushy (~15–55 vol% crystals) system that interacts with intruding melts from the mantle. These interactions result in disaggregation of crystal clots from the plutonic intrusives and remobilization of the crystals through various sub-environments of small ephemeral mush pockets. Eruption-triggering injections of melt then pick up these crystals with varied growth histories to be extruded.

## 1. Introduction

Magma is stored in reservoirs, defined as regions of partially or wholly molten rock containing varying proportions of melt, crystals, and exsolved volatiles (Bachmann and Bergantz, 2008), or as the domains of the magmatic system above the solidus that contain melt (± exsolved fluids) (Sparks et al., 2019). Magma reservoirs are compositionally and rheologically heterogeneous: following Hildreth (2004), we distinguish eruptible magmas with low (~0–5 vol%) to intermediate (~5–15 vol%) crystal contents from crystal mush (~15–55 vol%), a term coined by Wager et al. (1960), set in a rigid sponge of >55 vol% crystallinity. During storage, magmas, mushes and rigid sponges interact with freshly injected melts that alter the intrinsic compositional and rheological parameters of the storage region. Magma reservoirs are hosted by solid rocks, and in mature magmatic systems these constitute consanguineous plutonic intrusives that fully solidified from pre-existing melt pockets through ephemeral mushy and spongy states (Zellmer et al., 2024).

Crystals within the magma reservoir offer unique insights into the intrinsic conditions of the region. Changes in magma compositions and temperature (Bachmann and Dungan, 2002; Ginibre et al., 2007; Humphreys et al., 2006) as well as other open system processes such as mixing (de Maisonneuve et al., 2016; Degruyter et al., 2016; Ganne et al., 2018) result in chemical zoning of crystals, reflected in the distribution of major, minor, or trace elements in the minerals, and sometimes also in isotopic zoning (e.g. Ginibre et al., 2007; Kahl et al., 2011; Kahl et al., 2017; Mollo et al., 2020; Streck, 2008; Ubide et al., 2019a). Thus, variations in crystal chemistry provide a sensitive record of change over the lifetime of a crystal, from nucleation to final

* Corresponding author.
*E-mail address:* g.f.zellmer@massey.ac.nz (G.F. Zellmer).

https://doi.org/10.1016/j.chemgeo.2024.122333
Received 11 July 2024; Received in revised form 8 August 2024; Accepted 13 August 2024
Available online 14 August 2024

quenching (Holness et al., 2007a; Lange et al., 2013; Nielsen et al., 2020). However, not all changes promote crystal growth, they can also cause dissolution and breakdown of mineral phases. Therefore, textural features such as sieve textures, mineral breakdown, and resorption surfaces must be studied to fully understand the magmatic processes operating.

The characteristic behaviour of certain chemical elements is key to interpreting magmatic processes and transportation paths, based on the zonation of minerals. Petrological tools, such as thermobarometry and hygrometry, can be employed to reconstruct the conditions and processes that these crystals and the melt in which they are contained experienced in the subsurface (e.g., Mollo et al., 2010; Neave et al., 2019; Putirka et al., 1996). The crystal cargo is sensitive to variations in conditions such as pressure, temperature, oxygen fugacity ($fO_2$), composition of the host melt, and volatile content (Costa et al., 2013; Humphreys et al., 2006; Nakamura, 1995; Streck, 2008; Zellmer et al., 2003), as well as the degree of undercooling during their formation (MacDonald et al., 2023; Ubide et al., 2019b).

The origin of crystals and their relation to the host melt is key to understanding magmatic processes. Crystals are classified as autocrysts, antecrysts, and xenocrysts based on their genesis (Zellmer, 2021). Autocrysts are defined as crystals that have crystallised from the melt they are carried by and are in equilibrium with the melt. Antecrysts are minerals that have crystallised from the same magmatic system but have not crystallised from the melt they are entrained in and may or may not be in equilibrium with the melt. Xenocrysts are minerals that have formed in different magmatic (and non-magmatic) systems and are thus completely unrelated to the host melt. These crystals are typically picked up by ascending melts and are commonly in disequilibrium with the melt. In some scenarios, where the crustal basement is of magmatic origin, it may be difficult to distinguish between antecrysts and xenocrysts (Streck et al., 2007). Finally, as suggested by Zellmer (2021), we use the term phenocryst in its original meaning, namely a large crystal set in a fine-grained matrix (Iddings, 1892), without implying a petrogenetic origin.

Our previous work on Taranaki lava flows (D'Mello et al., 2023) focussed on the intensive parameters of the magmas prior to eruption, including temperature and volatile contents, using whole-rock, mineral, melt and bulk chemistry of a range of lava samples and their comparison to the mineral and bulk chemistry of cumulate xenoliths (Gruender et al., 2010; Price et al., 2016). These quantitative constraints led us to conclude that at Taranaki volcano, hot ($>1000$ °C), high-silica (up to 68 wt% $SiO_2$) melts sourced from the mantle pick up their mostly antecrystic or xenocrystic crystal cargo from cooler ($<1000$ °C), low-silica regions of the crust. In the present study, we extend this work by employing crystal imaging methods such as chemical mapping for major, minor and trace elements. We use the chemical and textural features of the crystal cargo of recent Taranaki lavas to gain insights into the long-term intrusive magmatic processes and conditions beneath Taranaki volcano. Specifically, we interrogate the crystal record to assess whether Taranaki volcanism is fed by a largely supersolidus and thermally buffered transcrustal magmatic system (Cashman et al., 2017), dominated by magmas, mushes, and rigid sponges where crystallization occurs at near equilibrium conditions; or alternatively by a mostly subsolidus system of plutonic nature recently suggested by (Coulthard Jr et al., 2024) for the southern Taupo Volcanic Zone to the East. In such transcrustal plutonic systems (Zellmer et al., 2024), small magma batches (Zellmer and Annen, 2008) are thought to be intruded into a cool crust, where they form ephemeral magma and mush pockets that rapidly transform to plutonic rocks. Here, rapidly ascending magmas that breach the surface entrain crystals that formed at low degrees of undercooling ($\Delta T < 50$ K) in spatially restricted mush pockets that rapidly solidified into small plutonic bodies.

To our knowledge, this is the first study that presents crystal chemical maps from eruptives of Taranaki volcano. We demonstrate that this method reveals a range of insights into the inner workings of this volcanic system that alternative methods have fallen short of providing.

## 2. Geological background and petrology

Mt. Taranaki is a near symmetrical stratovolcano on the western peninsula of the North Island of New Zealand (Fig. 1). It is the youngest and only active of three onshore volcanoes that form the Taranaki Volcanic Lineament (TVL). Seismic studies indicate that the crust-mantle boundary beneath the TVL is at a depth of *c.* 35 km (Sherburn and White, 2005). Insight into the rocks that form the crustal basement has been obtained from studies that focussed on the xenoliths entrained in the eruptive products of the TVL (Gruender et al., 2010; Price et al., 2021; Price et al., 2016). Mortimer et al. (1997) correlated xenolith and drill-core data from Taranaki to the Median Tectonic Zone in the South Island, suggesting that the *c.* 120 Myr old Median Batholith underlies the present-day edifices of Kaitake, Pouakai, and Taranaki (Fig. 1). Mt. Taranaki has been active for at least 130 kyr, and the current 12 $km^3$ edifice, erupted over the last ~8 kyr, represents only a small percentage of the volume of material extruded from the volcano (Alloway et al., 2005a; Procter et al., 2009; Zemeny et al., 2023; Zernack et al., 2011).

The long-term volcanic history includes at least 13 cycles of cone growth and collapse, with each collapse phase generating debris avalanche flows that form the extensive ring plain surrounding the volcano (Neall et al., 1986; Palmer and Neall, 1991; Zernack et al., 2011; Zernack and Procter, 2021; Zernack et al., 2009). Edifice reconstruction then follows through eruptions that range from explosive to effusive, generating volcanic products such as pyroclastic deposits, lava flows, and dome extrusions (Damaschke et al., 2017; Lerner et al., 2019; Platz, 2007; Platz et al., 2006; Turner et al., 2009; Turner et al., 2011; Turner et al., 2008).

The eruptive products of Mt. Taranaki considered for this study range from dense to scoriaceous lavas that form the current edifice of the volcano and are approximately 8 kyr in age. Basaltic trachyandesites are the predominant lithology, along with basalts and basaltic andesites (D'Mello et al., 2023). Variable proportions of crystals (35–55 vol%) are hosted in fine-grained groundmass (D'Mello et al., 2023). These phenocrysts are up to 4 mm in size and are dominated by plagioclase, clinopyroxene, amphibole, and opaque minerals (Fe-Ti oxides). In rare cases, orthopyroxene and olivine are seen in the groundmass. Accessory mineral phases include biotite and apatite. Glomerocrysts are common and comprise intergrown clinopyroxene ± plagioclase, magnetite, and amphibole crystals. The groundmass phases include plagioclase, pyroxene, and oxide microlites with interstitial glass (< 5 vol%). Mantle normalised trace element pattern for whole rock data show typical 'arc' signatures with enriched large ion lithophile element (LILE) contents and high LILE to high field strength element (HFSE) ratios, as well as high light rare earth element (LREE) to heavy rare earth element (HREE) ratios (D'Mello et al., 2023).

## 3. Methodology

Samples were selected from lava flows representing different stratigraphic units and whole rock compositions ranging from basalts to trachyandesites. Following Zellmer (2021), major phenocryst phases of plagioclase, clinopyroxene, and amphibole (if present in the sample) were classified by size as microcrysts (>30 μm width and < 100 μm length), mesocrysts (100–500 μm length), and macrocrysts (500 μm–10 mm length), which in Taranaki are set in a fine-grained matrix rich in microlites (1–30 μm width).

### 3.1. Back scattered electron (BSE) imaging

Representative samples were cut and polished at Massey University, New Zealand. Polished sections were coated using a carbon sputter coater at the Manawatu Microscopy Imaging Centre. The sections were then viewed using a BSE detector attached to a FEI 200 Quanta Scanning Electron Microscope (SEM) at the Manawatu Microscopy Imaging Centre. An accelerating voltage of 20 kV and a working distance of 10

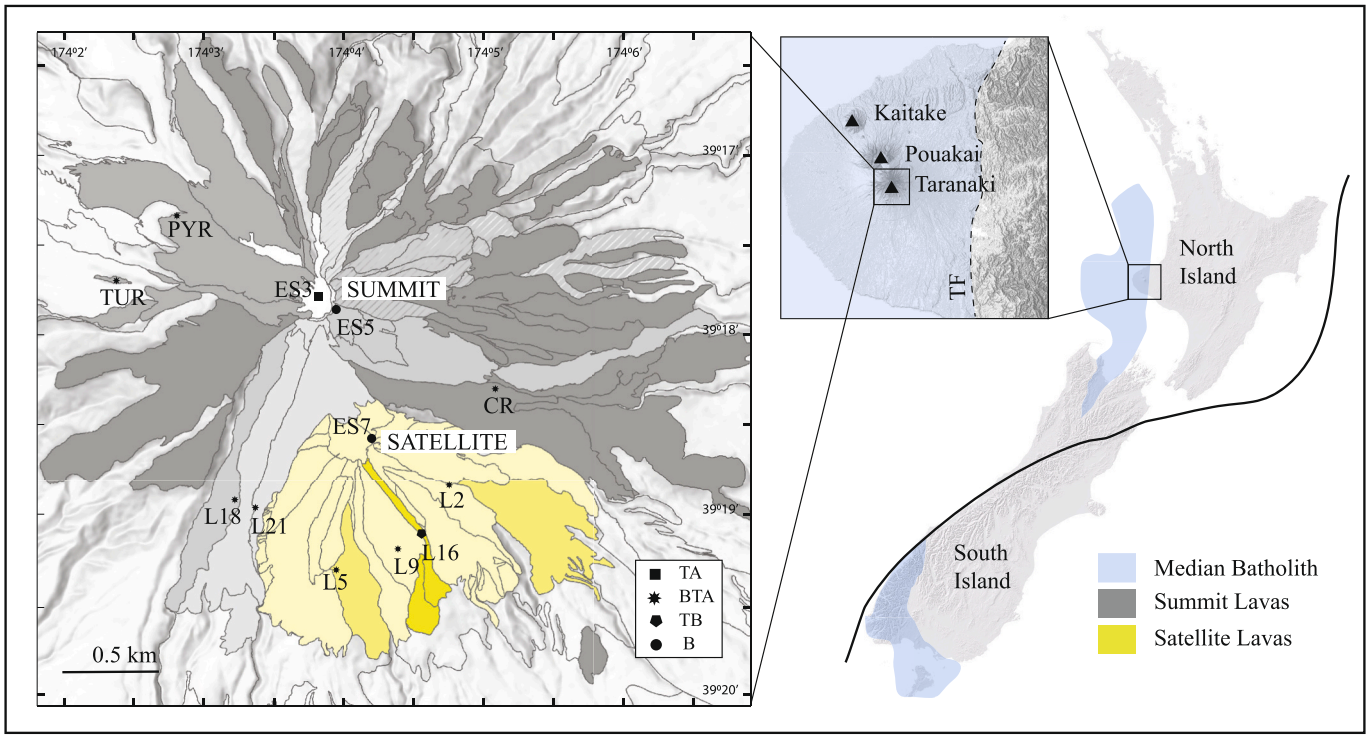


**Fig. 1.** (A) Map demarcating the lava flows of Taranaki volcano erupted from the summit and satellite vent and the location of samples used in this study. Darker tones correspond to older eruptions. TA: Trachyandesite; BTA: Basaltic trachyandesite; TB: Trachybasalt and B: Basalt. (B) Map of New Zealand showing the trace of the convergence of the Indo-Australian plate and the Pacific plate. Blue shaded region represents the extent of the Median Batholith, which forms part of the basement of Taranaki volcano. Inset shows the Taranaki Volcanic Lineament (TVL) and the location of the three onshore peaks younging towards the Southeast with Taranaki being the youngest edifice. TF shows the trace of the Taranaki Fault. (For interpretation of the references to colour in this figure legend, the reader is referred to the web version of this article.)

mm was maintained. Spot analysis to identify mineral phases was conducted using Genesis EDAX software and considering the relative counts per second of Ca, Al, Mg, and Si. Images obtained were imported into ImageJ and adjusted for contrast and brightness.

### 3.2. Electron probe micro-analysis (EPMA) mapping

Major oxide chemical mapping of minerals was performed using a JEOL W-EPMA JXA-8900R microprobe at the laboratory for electron and X-ray beam analyses, Institute of Earth Science, Academia Sinica in Taipei, Taiwan. 26 clinopyroxene, 16 amphibole, and 37 plagioclase crystals were selected and represent the temporal and spatial variations of the Taranaki lavas. Clinopyroxene crystals were mapped for Al, Mg, Si, Na, and Ca; amphibole for Al, Mg, Si, Na, K, Fe, Ca, Ti; and plagioclase was mapped for Si, Na, K, Al, Ca. Elemental distribution images were obtained with 15 kV of accelerated voltage and 50 nA of beam current with a 2 μm de-focused beam and 20 ms of dwell time. X-ray intensities were measured in intervals of 5 μm. The maps were then set to the same colour scale as LA-ICP-MS maps using the 'Lookout Table" tool in ImageJ. Quantitative spot analyses on each crystal were done to obtain major oxide compositions of the crystal. X-ray intensity maps for the major elements obtained were calibrated to one or two EPMA quantitative spot analyses per crystal to obtain semiquantitative maps for major element concentrations in wt% as well as Mg# [defined here as 100 × molar $Mg/(Mg+Fe^T)$] for clinopyroxene and amphibole) and anorthite (An) content (for plagioclase), using Fiji ImageJ software. This was accomplished by using the 'calibration tool' and setting 0 intensity to 0 wt%, and spot intensity to the quantitative wt% using a linear function.

### 3.3. Laser ablation inductively coupled plasma mass spectrometry (LA-ICP-MS) mapping

Trace element compositions and zoning patterns of minerals were investigated following the rastering technique of Ubide et al. (2015). Runs were carried out at the University of Queensland Centre for Geoanalytical Mass Spectrometry, Radiogenic Isotope Facility (UQRIF-lab). The instrument employed was an ASI RESOlution 193 μm eximer UV ArF laser ablation system with a dual volume Laurin Technic ablation cell and GeoStar Norris software, coupled with a Thermo iCap RQ quadruple mass spectrometer operated by Qtegra software. The laser was run at 1.0 kV with a repetition rate of 10 Hz, yielding an energy of 4 mJ. Laser spot size was adjusted to 10 μm through an exit slit, and the stage was moved to obtain a scan speed of 10 μm $s^{-1}$ with a trace overlap of 5 %, yielding a fluence of 2.0 J $cm^{-2}$. Ablation was performed in ultrapure He to which Ar make-up gas with trace amounts of $N_2$ was added for efficient transport and to aid ionization. The instrument was tuned with scans on NIST SRM 612. Elemental maps were built using Iolite (Paton et al., 2011) v2.5 in quantitative mode, using NIST 612 glass reference material as the calibration standard and Ca concentrations in the case of clinopyroxene (cpx) and amphibole (amp) and Si concentrations in the case of plagioclase (plg), obtained by EPMA, as internal standards. Secondary standards BCR-2G and BHVO-2G were analysed regularly during the run to monitor data quality. Precision was typically better than 5 % for all measured elements and accuracy better than 10 %.

## 4. Results

The crystal cargo of Taranaki lavas shows disequilibrium textures such as sieve textures and resorption surfaces, as well as normal, reversed, and oscillatory zoning. Fine-scale zoning patterns are best observed in BSE images due to their higher resolution compared to that

of LA-ICP-MS maps (Fig. 2 and supplementary material S1). EPMA and LA-ICPMS chemical maps of crystals are provided as supplementary materials S2 and S3, respectively, and selected maps are provided here for plagioclase (Fig. 3), clinopyroxene (Figs. 4 and 5), and amphibole (Fig. 6). These phases are discussed in turn below. In the present study, we did not observe any systematic variation of the petrographic features with bulk rock chemistry.

### 4.1. Plagioclase

Plagioclase is the most abundant mineral phase in the Taranaki lavas ranging from 25 to 45 vol% and is found as macrocrysts, mesocrysts, and microcrysts. Texturally, the microcrysts are generally euhedral, while the larger crystals are often subhedral to subrounded with sieve textures (Fig. 2 A-C). Plagioclase compositions range from labradorite ($An_{40}$) to anorthite ($An_{92}$), where the An-number is calculated as 100 × molar Ca/(Ca + Na + K). Despite the textural variation observed, the classification of plagioclases can be based on the presence and composition of a distinct core shown by most crystals ($n$ = 32 of 36), enveloped by a mantle and rim (Fig. 3).

The An content of the cores in relation to the mantle and rim further classifies them as: (i) normal zoned with a high An core and an oscillatory mantle and rim with progressive decrease in An ($n$ = 22), (ii) reverse zoned with a low An core that is usually rounded and a high An mantle that is often associated with sieve texture ($n$ = 4), (iii) a patchy zoned core with an oscillatory zoned mantle and rim ($n$ = 6), (iv) a normally zoned crystal without the presence of a distinct core but a gradual decrease in An from its centre to the rim (n = 4). Microlites are normally zoned with no evidence of disequilibrium textures. Commonly, the outermost rim of the larger crystals corresponds to the An content of

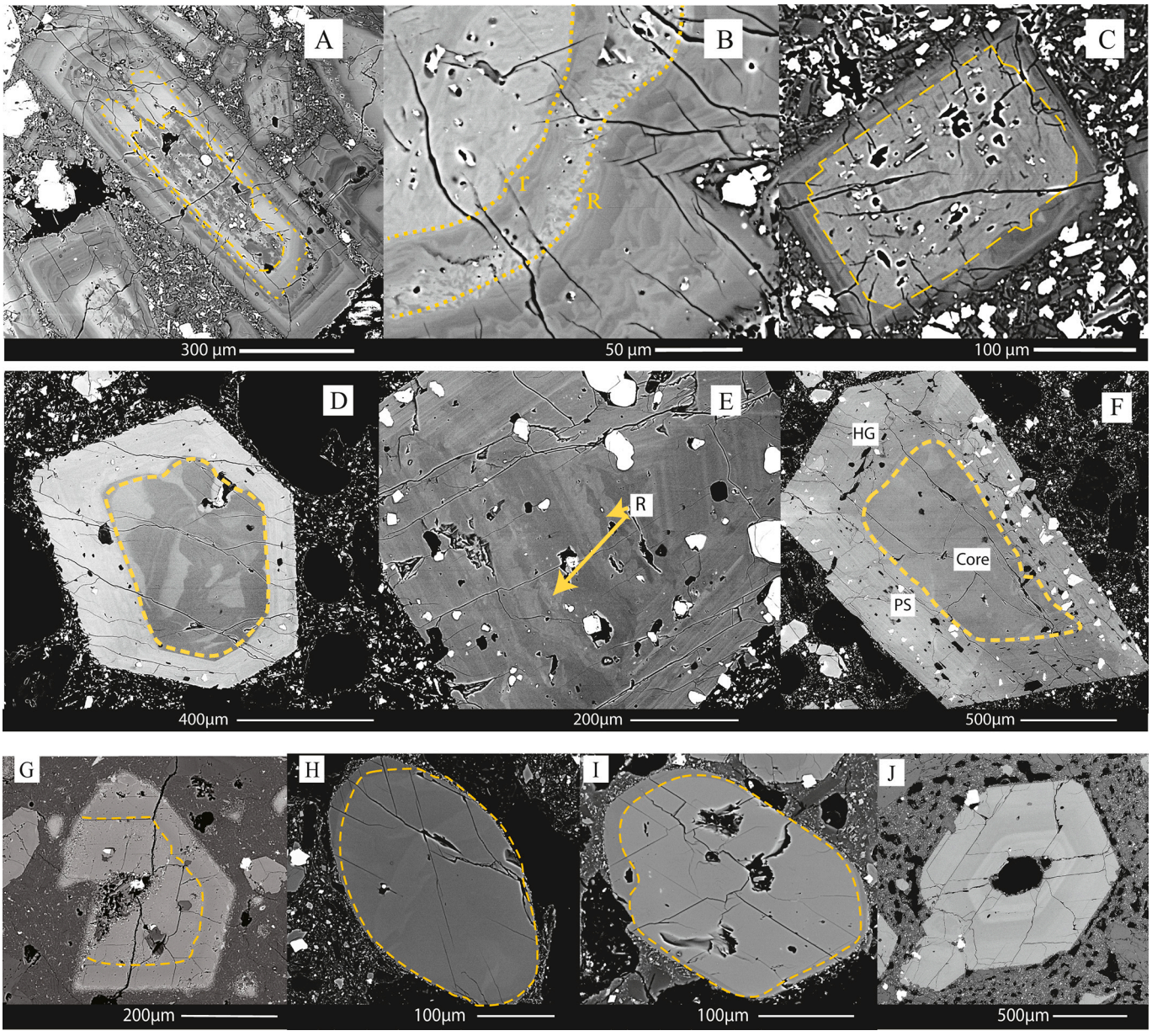


**Fig. 2.** Panel 1 shows the different types of textures in plagioclase: (A) patchy core, (B) minor (r) and major (R) resorption surface and wavy oscillatory zoning; (C) cellular and sieve texture. Panel 2 shows clinopyroxene textural features: (D) patchy zoned core and oscillatory zoned mantle; (E) wavy oscillations in the hourglass sector and straight oscillations in the prism sector with resorption surface (R); and (F) distinct patchy zoned core and sector zoned mantle showing hourglass (HG) and prism (PS) sectors. Panel 3 shows textures in amphibole: (G) euhedral core with mantle and reaction rim, (H) rounded patchy core and thin rounded rim, (I) unzoned large core and mantle, and (J) oscillatory zoned crystal with completely resorbed core.

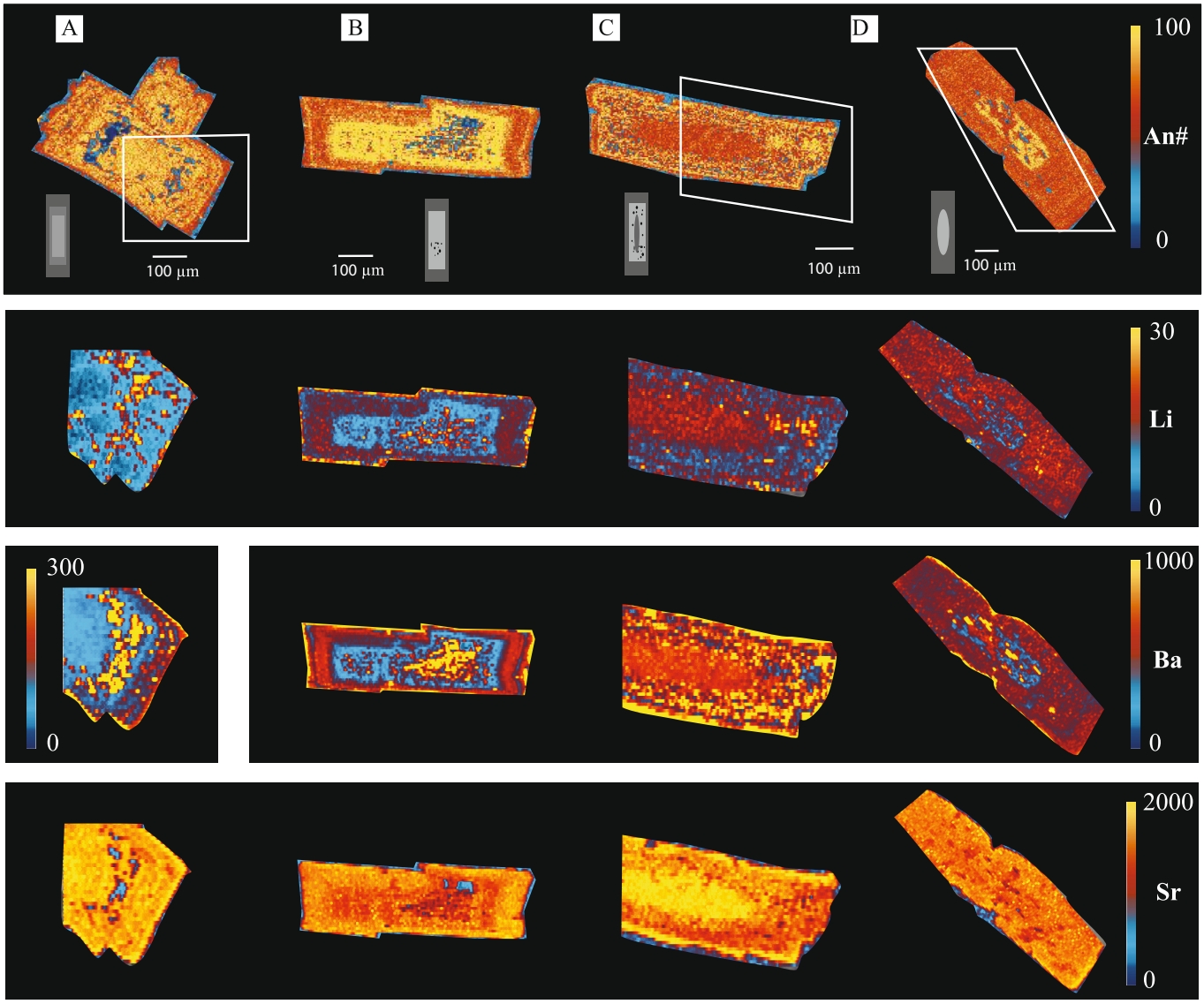


**Fig. 3.** Types of zoning seen in plagioclase of Taranaki lavas. (A) Normally zoned crystal with a sieved mantle and oscillatory zoning from sample L16; (B) An-rich, distinct core with sieved interior and oscillatory zoned mantle from sample ES3; (C) reverse zoned crystal with an An-poor core and sieved mantle from sample PYR; (D) normally zoned crystal with patchy core and oscillatory zoned mantle from sample PYR. Graphs show profile values for elements Li, Ba and Sr from core to rim (in µg/g). Refer to Fig. 1 for sample locations.

the microlites in the EPMA maps (see supplementary material S2).

Along with patchy zoned cores, some cores show high An with box-like patches of low An that have been described as cellular textures (Van Gerve et al., 2020) and vary from boxy to rounded or irregular in shape. The oscillatory zoned mantles contain numerous low amplitude cyclic zones and are associated with resorption features that appear wavy in BSE images (Fig. 2). Sieve texture bands in the core and mantle are associated with lighter BSE image tones, indicating higher An content. The mantles are usually euhedral and are overgrown by a thin, euhedral rim.

Taranaki plagioclase crystals are also distinguished based on zoning of trace elements Ba, Sr, and Li (Fig. 3). Step zoning is commonly observed in most crystals, where the change in composition is abrupt, demarcating a core. Ba zonation typically compliments An, thereby demarcating cores, oscillatory zoned mantles, and rims. Sr zonation shows both positive and negative correlations to An contents, but also displays flat profiles in some crystals. The zoning patterns observed for Li concentrations in the plagioclase crystals can be flat, high in the cores, or high in the rims/mantles, and with a few exceptions are broadly anticorrelated with An-content.

### 4.2. Pyroxene

Major element compositional data for all clinopyroxene crystals from Taranaki classify as diopsides and augites based on the classification scheme of Morimoto (1988). Clinopyroxene (cpx) commonly occurs as zoned, euhedral macrocrysts, large crystal clots, and normally zoned microlites in the groundmass. Clinopyroxenes have a narrow range of Mg# between 73 and 85 (Fig. 4). The clinopyroxenes of Taranaki contain low concentrations of Cr, consistent with the low Cr content of the whole rock compositions (D'Mello et al., 2023).

The most common type of zoning is oscillatory zoning, characterised by multiple, concentric growth layers in the mantles (e.g., Fig. 5A). Zones along the prism faces {110,100,010} show scarcely resorbed, parallel oscillatory zoning, while in the hourglass sector they are generally thicker. Crystal rims are narrow and show euhedral outlines.

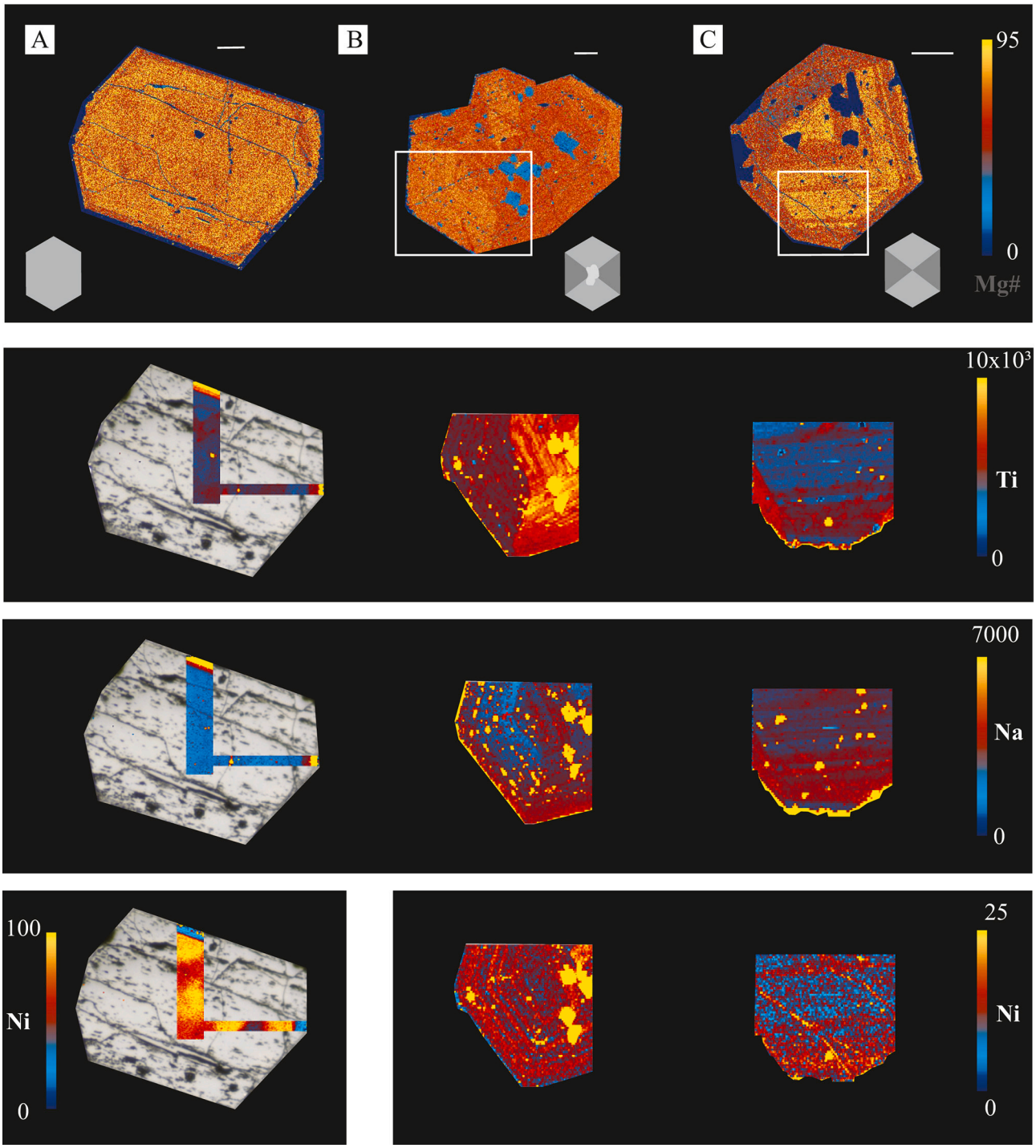


**Fig. 4.** Types of zoning seen in clinopyroxene of Taranaki lavas. (A) Patchy zoned core with low Mg# mantle and high Mg# rim from ES5; (B) sector-zoned crystal showing Mg-Si rich hourglass sectors and Al-Ti rich prism sectors, also present is a resorbed core from L2; (C) sector zoned crystal cut oblique to the c-axis without distinct core, from sample L5. Panels show relative concentration of elements Na, Ti, Ni and Zr (in μg/g) from core to rim. Refer to Fig. 1 for sample locations.

Clinopyroxenes were categorised based on the presence of chemically distinct cores, which appear anhedral and resorbed with a sharp interface with the mantle. The following three types were found (supplementary materials S1 and S3): (i) no distinct core observed for the intersect ($n$ = 15 of $n$ = 24), (ii) a distinct unzoned core present and identified for all elements ($n$ = 6), and (iii) large patchy zoned core with thin mantle and rim ($n$ = 3).

Most cpx crystals ($n$ = 21) show sector zoning of the mantles, chemically divided into prism and hourglass sectors (Fig. 2 D-F). These sectors are characterised by oscillatory zoning to form euhedral crystal outlines. Sector zoning is characterised by preferred uptake of Si and Mg in the hourglass sector and preferred uptake of Ti (Fig. 4), Al (Fig. 5), rare earth elements (REEs), and Zr in the prism sector, while most transition elements do not show sector zoning. Partitioning of elements in four crystals with sector zoning from different lava flows is represented in Fig. 5. It is observed that the difference in major oxide ($SiO_2$, MgO and $Al_2O_3$ in wt%) and trace element (Ti and Zr in μg/g) is comparable between samples although they are hosted by melts of varying compositions.

Clinopyroxenes zoning patterns can be defined for key elements such

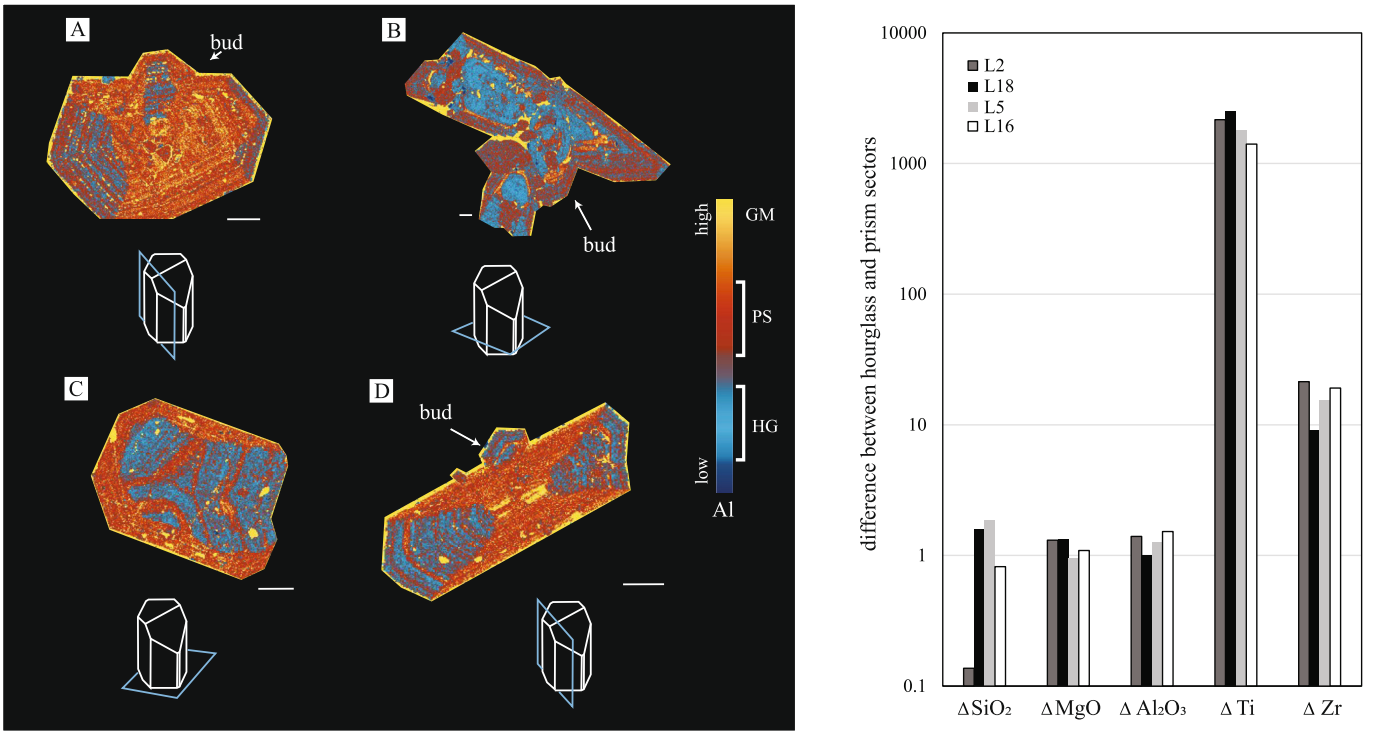


**Fig. 5.** Sector-zoned clinopyroxenes from samples (A) L2; (B) L18; (C) L5 and (D) L16. The white scale bar represents 200 μm. Crystal outlines show the intersect of the crystals, which results in the sector patterns observed. The graph illustrates the comparable partitioning difference of oxides and elements between the hourglass (HG) and prism (PS) sectors. Hourglass sectors are enriched in $SiO_2$ and MgO, while the prism sectors are enriched in $Al_2O_3$, Ti and Zr. $SiO_2$, MgO and $Al_2O_3$ are in wt %, while Ti and Zr are in μg/g. Groundmass $SiO_2$ for the host lavas are (in wt%): L2 = 62.6; L18 = 64.4; L5 = 60.6; L16 = 60.7. Refer to Fig. 1 for sample locations.

as Na, Mg and Fe; transition elements (Cr, Ni and Sc), rare earth elements (La), and Zr. Na displays weak sector zoning and when present, the cores either show lower or higher Na concentration as compared to the mantles and rims. In contrast, crystal mantles are strongly sector zoned for Al, Ti, La, Zr, V (enriched in prism sectors) and Mg# (enriched in hourglass sectors) (Fig. 4; supplementary material S3). Cr concentrations are relatively low and enriched zones are rare, however when present crystals show either an enriched core, multiple/single enrichment zones in the mantle or an enriched rim. Sc and Ni zonations are more common and define cores rarely reflected by the major elements.

### 4.3. Amphibole

Amphiboles found in Taranaki lavas are calcium-rich and are classified as pargasites (Hawthorne et al., 2012). Amphiboles are not present in all the samples and their abundances vary between samples of the same lava flow. Reaction rims and regions of decomposition are characterised by the replacement of amphibole with anhydrous phases including plagioclase, orthopyroxene, clinopyroxene, and oxides (for details on reaction breakdown features, see D'Mello et al., 2021).

Based on BSE images and intracrystalline variations of the Mg# of the crystals, the amphiboles were categorised as (i) unzoned ($n = 5$), (ii) normal zoned with a high Mg# distinct core and a lower Mg# oscillatory zoned mantle ($n = 3$), and (iii) oscillatory zoned ($n = 9$) (Fig. 2 G-J). Oscillatory zoning is characterised by cyclic changes in greyscale with no abrupt interface, but rather a diffuse contact between zones. Major element zonation is weak, except for Al. However, minor and trace elements show stronger variations in the crystal from core to rim. Amphibole zoning was further characterised using Ni, V, La, Ce. Cr, Ni and V, which show similar enrichment patterns, although Cr concentrations are often too low to quantify (Fig. 6).

## 5. Discussion

In the following, we first discuss the variety of mineral textures seen in Taranaki lavas, indicating how such textures have been interpreted previously. We then turn to the crystallization environments operating beneath Taranaki, based on those textural and mineral chemical constraints. In each of these first two subsections, plagioclase, pyroxene and amphiboles are addressed consecutively. Subsequently, we discuss the origin of the crystal cargo as a whole based on these interpretations, and close with the a section on the petrogenesis of the lavas that form the current Taranaki volcano edifice.

### 5.1. Mineral textures

#### 5.1.1. Plagioclase

*Sieve textures.* Sieve textures are common in the plagioclase of volcanic rocks and mantle xenoliths, and can develop as a result of changes in temperature, pressure or melt compositions (Humphreys et al., 2006; Nelson and Montana, 1992; O'Brien et al., 1988; Pan et al., 2018; Stewart and Pearce, 2004; Tomiya and Takahashi, 2005). In Taranaki samples, sieve textures in plagioclase are associated with higher An contents indicative of interaction of the crystal with hotter, more mafic magma compositions (based on experiments on plagioclase dissolution, cf. Tsuchiyama, 1985; Fig. 2C). This interaction resulted in the partial dissolution of the crystal and recrystallization of plagioclase in equilibrium with the new environment. The relative location of the sieve textures within the crystals is variable: some are found in the cores, but most are associated with the mantles, usually preceded by patchy zones and the formation of resorption surfaces (Fig. 2B).

*Patchy Zoning:* The development of patchy textures in the cores of plagioclase crystals is interpreted as the result of partial dissolution and regrowth (Ginibre and Wörner, 2007; Humphreys et al., 2006). In the Taranaki samples, the low An patches are few and disconnected and are

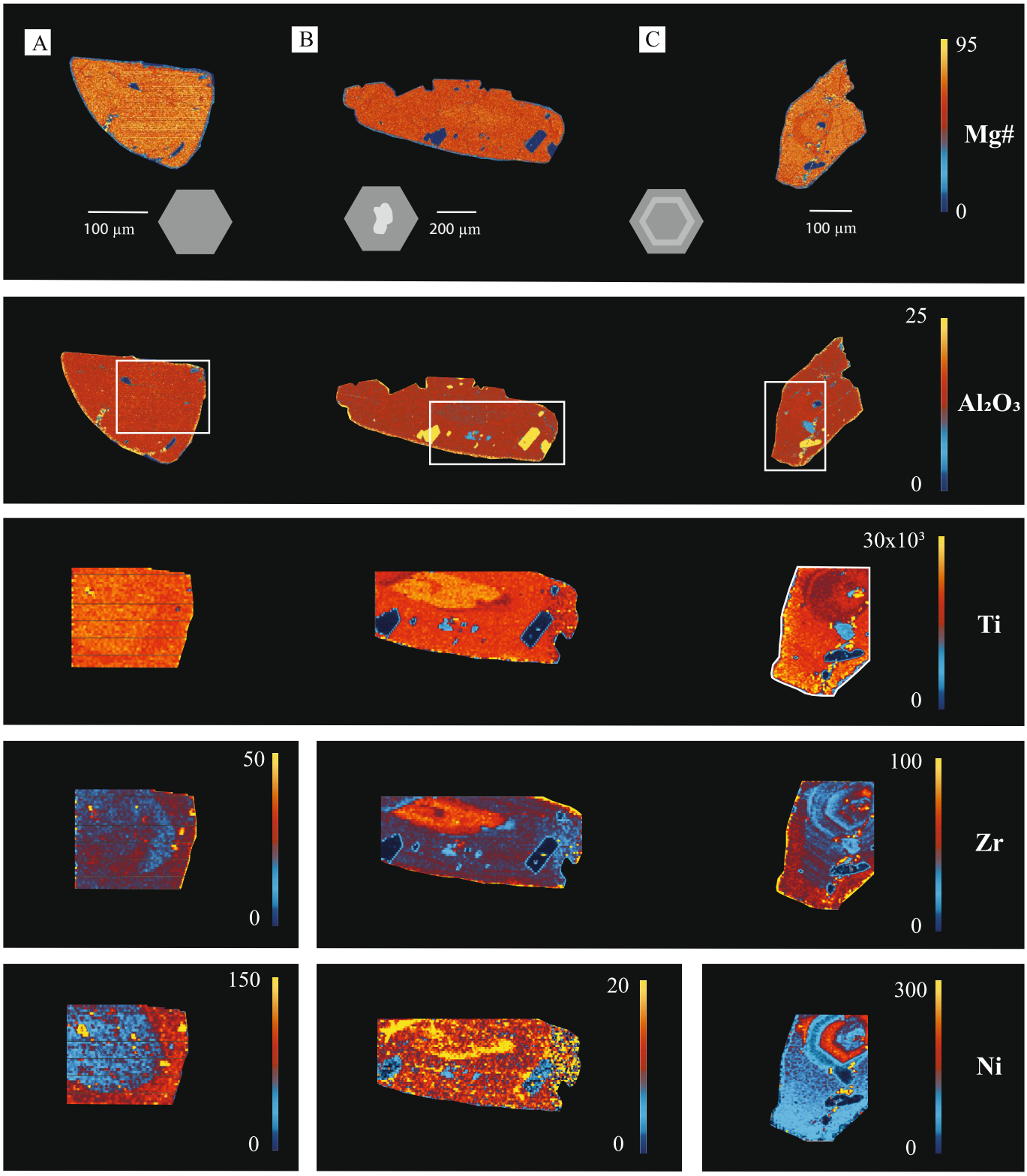


**Fig. 6.** Types of zoning seen in amphiboles of Taranaki lavas. (A) Unzoned crystal from ES3; (B) high Mg# core and low Mg# mantle from L5; (C) high Mg# crystal with low Mg# but high Cr mantle resorption interface from L16. Panels show relative concentration of $Al_2O_3$ (in wt%), and elements Ti, Zr and Ni (in µg/g). Refer to Fig. 1 for sample locations.

typically completely enclosed within a high-An euhedral core (Fig. 2A). To produce this texture, resorption of low An plagioclase followed by growth of high An plagioclase is required. In addition, Fe maps obtained from LA-ICP-MS show very little variation despite large changes in An content, indicating that no significant compositional change of the melt occurred. This suggests that the early An-poor patches were overgrown by An-rich zones that precipitated immediately after dissolution (Humphreys et al., 2006; Nicotra and Viccaro, 2012). A regular supply of mafic magma infiltrating a more evolved crystal mush, or the transport of the crystals into a region where the pre-existing melt was in

equilibrium with higher-anorthite plagioclase may result in patchy zoned crystals (cf. Van Gerve et al., 2020).

*Cellular texture.* Cellular textures are different from sieve and patchy cores and are attributed to the skeletal growth of disequilibrium, low An plagioclase followed by infilling and overgrowth by higher An plagioclase (Fig. 2C) (Bennett et al., 2019; Nakamura and Shimakita, 1998; Tsuchiyama, 1985). The low An area in the cellular textural zones are remnants of the partially dissolved skeletal plagioclase, and higher-anorthite cells represent channel sections along which dissolution–reprecipitation of high An plagioclase occurred.

*Resorption Surfaces.* The macrocrysts in this study show clear major and minor wavy surfaces, which erode previous growth layers and are indicative of resorption. In plagioclase, this is characterised by gradual decrease of An content and a sharp increase across the next resorption surface (Fig. 2B). Temperature, magma composition, and volatile content have the greatest effects on plagioclase stability and composition, and small fluctuations can induce resorption events (Almeev et al., 2012; Grove et al., 1992; Moschini et al., 2023; Namur et al., 2012; Tsuchiyama, 1985). Resorption of plagioclase occurs either upon a change in magma chemistry (Nakamura and Shimakita, 1998; Tsuchiyama, 1985), an increase in temperature (Johannes et al., 1994), a decrease in pressure (Nelson and Montana, 1992; Vance, 1962) or a combination of changes in the system. Increasing temperature would result in crystallization of An-rich plagioclase (Grove et al., 1992; Namur et al., 2012). However, diverse primary melts reported for Taranaki (D'Mello et al., 2023) can supply low-An melts as well as remobilize the crystal cargo into more felsic parts of the subvolcanic system with consecutive injections. In addition, infiltration of interstitial melts in crystal mushes may lead to reactive dissolution of minerals (Coogan et al., 2000; Lissenberg and MacLeod, 2016).

*Oscillatory Zoning.* There are two possible causes for the formation of oscillations of chemistry during crystal growth: (1) extrinsic causes such as changes in pressure (P), temperature (T) or magma composition (X); or (2) intrinsic causes such as fluctuations between diffusive and advective supply of cations in a melt boundary layer immediately adjacent to the growing crystal (Alloway et al., 2005b; Schoneveld et al., 2020; Shore and Fowler, 1996; Streck, 2008). Short-wavelength (1–10 μm) oscillations (Fig. 2A) are common in clinopyroxene and plagioclase and are attributed to growth kinetics, magma recharge events and convection processes (Ginibre et al., 2002a; Ginibre et al., 2002b; Humphreys et al., 2006; Tsune and Toramaru, 2007). Kinetic models and detailed microanalytical observations (Zellmer et al., 2016) indicate that high crystal growth rates result in the formation of a boundary layer, in which elements become depleted when mineral growth rates exceed the diffusive supply of elements from the melt. Alternatively, repeated, small volume injections of melt of different compositions can also form oscillatory zoning.

### 5.1.2. Clinopyroxene

*Sieve texture.* Neave and Maclennan (2020) show that sieved cores in clinopyroxenes can be indicative of rapid ascent dissolution of clinopyroxene (Figs. 2E, F). High Al content in the clinopyroxene is indicative of high-pressure crystallisation. During rapid ascent, decompression-driven dissolution of $Al_2O_3$-rich cores is followed by low-$Al_2O_3$ overgrowth forming the rim. However, relative to the mantles and rims, the sieved cores of Taranaki clinopyroxenes have a similar range in Mg# and low $Al_2O_3$. They are thus unlikely to have formed by rapid decompression. Instead, the sieved cores may be attributed to the partial dissolution of early formed low $Al_2O_3$ cores by melt, now reflected in the groundmass, at the onset of eruption, although volatile flushing may also have contributed (Giuffrida et al., 2018).

*Patchy zoning.* The patchy zoning of clinopyroxenes also indicates intense dissolution of early crystallized clinopyroxene by fresh magma, as evidenced by the presence of abundant melt inclusions in the high-Mg#, dark domains of the patchy zones. However, the contacts of patches of different Mg# appear diffuse, indicating prolonged residence at elevated temperature may have resulted in Fe-Mg interdiffusion (Fig. 2D).

*Sector zoning.* Clear Si- and Mg-rich hourglass sectors, and Al, Ti and REE rich prism sectors (Fig. 5) are observed in some but not all (Fig. 4A) Taranaki clinopyroxenes. This type of zonation is common in natural terrestrial (Downes, 1974; Hollister and Gancarz, 1971; Leung, 1974; Ubide et al., 2019b; Welsch et al., 2016), lunar (Hollister and Gancarz, 1971) and experimental pyroxene (Lofgren et al., 2006; MacDonald et al., 2023; Masotta et al., 2020; Schwandt and McKay, 2006). These sector zones represent differences in chemistry of a crystal due to kinetic effects at the growth surface, whereby elements are incorporated into the structure at different rates along different crystallographic surfaces, rather than changes in chemistry or conditions of the surrounding magma (Hollister and Gancarz, 1971). There are at least four controlling factors for the creation of sector zones, as explained by Hollister and Gancarz (1971): (1) size and composition of ionic complexes added to the crystal as it grows, (2) rate of addition of material, (3) rate of equilibration of the new material with the matrix at the surfaces of growth steps, and (4) rate of re-equilibration of surface layers with the matrix by exchange of ions perpendicular to the crystal faces. Sector zoning is formed at low degrees of undercooling with $\Delta T < 50$ K (Colle et al., 2023; MacDonald et al., 2023; Masotta et al., 2020), which could be a result of regular degassing of the magma reservoir, magma mixing and/or crystal movement between the hot interior and cold margin caused by magma convection (Ubide et al., 2019b). In contrast, experimental evidence shows very high degrees of undercooling produce rapid hopper or skeletal crystals that may become subsequently infilled overgrown (MacDonald et al., 2022; Masotta et al., 2020; Pontesilli et al., 2019). No distinct skeletal or dendritic zoning with regular fine layers is observed in Taranaki crystals, indicating a crystallisation environment close to thermal equilibrium and growth or oscillatory-zoned to sector-zoned crystals at low degrees of undercooling. Sector-zoned crystals across different samples show similar variations of $SiO_2$, MgO, $Al_2O_3$, Ti and Zr between the hourglass and prism sectors (Fig. 5), suggesting that the crystals formed in similar undercooling environments (MacDonald et al., 2024).

*Resorption surfaces.* Clinopyroxenes also show overgrowth of a single layer with a sharp resorption surface (Fig. 2E), attributed to a change of melt composition during crystallization (Ginibre et al., 2002a; Ginibre et al., 2002b). These resorption surfaces are categorised as major resorption surfaces (high amplitude oscillation), while minor resorption surfaces (low-amplitude oscillation) are attributed to local mixing of magmas with less contrasting compositions (Elardo and Shearer, 2014; Ginibre et al., 2007). Therefore, the resorption surfaces in clinopyroxene are the result of variable degrees of magma or crystal-melt mixing. The major and minor resorption surfaces are sometimes associated with either high Mg# and high Cr or low Mg# and low Cr oscillations, indicating multiple recharging events involving primitive or evolved magmas during the growth of a crystal.

### 5.1.3. Amphibole

*Resorbed cores.* Amphiboles are euhedral to subhedral (Figs. 2G, I). Compatible elements like Ni show enriched zones indicative of mafic recharge events occurring between the crystallization of the core and the rim. The concentration changes in elements such as Ti and Zr from the resorbed core and the rim can in principle be explained by processes of fractional crystallization or magma mixing. The sharp boundaries between cores and rims indicate the sudden entrainment of the crystal in a magma of different compositions. Reversals of zoning are also observed. For example, Fig. 6A shows a high Ni rim, indicating mixing with mafic magma at a later stage of crystallization, while Fig. 6B shows a core with enriched Ni, indicating an initial mafic crystallization environment. These alternations of crystallization environments support magma mixing over fractional crystallization, where the boundaries would be less well defined, and the zoning would be normal. Details on the stability of amphibole in mafic arc magmas and associated reaction

textures can be found in D'Mello et al. (2021).

#### 5.1.4. Glomerocrysts

Glomerocrysts are abundant in Taranaki lavas, and several optical microscopy images are provided in supplementary material S4. They may either have formed through heterogeneous nucleation followed by overgrowth, as e.g. seen from experimental work by Colle et al. (2023), or they are remnants of disintegrating igneous xenoliths as typically seen in continental arc environments (Zellmer et al., 2024). We prefer the latter interpretation, as texturally these glomerocrysts are variable and do not mirror the dendritic growth around single nuclei seen in experimental charges. Further work on the Taranaki glomerocrysts will be required, however, to fully understand their genesis, because they were not subject to the detailed mineral chemical work of the phenocrysts we targeted in the present study.

### 5.2. Crystallization environments: insights from chemical mapping

#### 5.2.1. Plagioclase

*Inferences from anorthite zoning.* Changes in melt composition, temperature, and pressure are recorded in the compositional zonation of plagioclase crystals (Bowen, 1913; Drake, 1976; Longhi et al., 1993; Putirka, 2008; Waters and Lange, 2015). If zones of similar composition exist among different crystals, it is reasonable to assume that they crystallized in similar magmatic environments at comparable pressure, temperature, and composition conditions (e.g. Kahl et al., 2011; Mollo et al., 2015; Viccaro et al., 2016). In Taranaki samples, we identify plagioclase zones with 50–70 and 75–90 mol% An ranges (Fig. 7), which distinguish the low An and high An environments of crystallisation. The various types of plagioclase crystals observed can be explained by crystallisation in one environment, followed by the introduction of the crystal into a new environment and the subsequent resorption, dissolution and recrystallisation. Formation of crystals in a felsic environment results in a low An core that is then introduced into an environment of high An content. This leads to the dissolution and resorption of the crystal, forming sieve textures or rounding of the core (Fig. 7A). If resorption is complete, only a sieve portion of the core may be left, and the core of the crystal appears An-rich (Fig. 7B). In this new An-rich environment, An-rich cores of new crystals form and then these crystals are introduced into a new An-poor environment, indicated by a sharp boundary where they may reside for long (Fig. 7C) or short (Fig. 7D) periods.

These sub-environments within the subvolcanic system can be attributed to (i) repeated, small volume, injections of diverse melts into a crystal-rich sponge or plutonic body, and/or (ii) transportation of crystals between different sub-environments. A combination of these processes results in a plagioclase population with varied histories and zoning types over short length scales that would not have been possible if the crystals had grown *in situ*.

*Inferences from Sr and Ba zoning.* Incorporation of Ba and Sr in the plagioclase crystal lattice are a result of Ca substitution, i.e., is strongly dependent on An content, with subordinate influence of crystal structure, melt composition, and temperature (Bindeman et al., 1998; Blundy and Wood, 1991; Giletti and Casserly, 1994). If major-element zoning patterns are preserved, the equilibrium concentration of Sr and Ba obtained after diffusion in the crystal are inversely correlated with An content (Coulthard Jr et al., 2024; Zellmer et al., 1999). The variable Ba and Sr concentration at high An content in Taranaki lavas reflects the influence of different initial magmas combined with long storage in a cool environment to preclude diffusive equilibration of these trace elements.

*Inferences from Li zoning.* Lithium is a moderately incompatible element in plagioclase ($K_D \sim 0.15–0.7$), as determined by experimental data covering a range of temperatures (1153–1299 °C) and anorthite contents ($An_{39–77}$) (Bindeman and Davis, 2000; Bindeman et al., 1998; Giletti and Shanahan, 1997). The crystals from Taranaki lavas that we imaged confirm incompatibility: the concentration of Li in melt inclusions, cracks and the matrix surrounding the crystals yield higher Li-contents than the crystals. Further, more recent experimental results of Coogan (2011) indicate that the Li is more compatible in sodic plagioclase than calcic plagioclase within the compositional range of $An_{60–90}$. This should produce an anticorrelation of Li and An# or Ca in plagioclase, and with few exceptions this is indeed observed for Taranaki crystals (Fig. 3 and supplementary material S3).

Rapid diffusion of Li at magmatic temperatures (Cherniak, 2010; Giletti and Shanahan, 1997) can modify Li zoning during syn- and post-eruptive degassing or regassing (Berlo et al., 2004; Blundy et al., 2008; Charlier et al., 2012; Coogan, 2011; Ellis et al., 2018; Genareau and

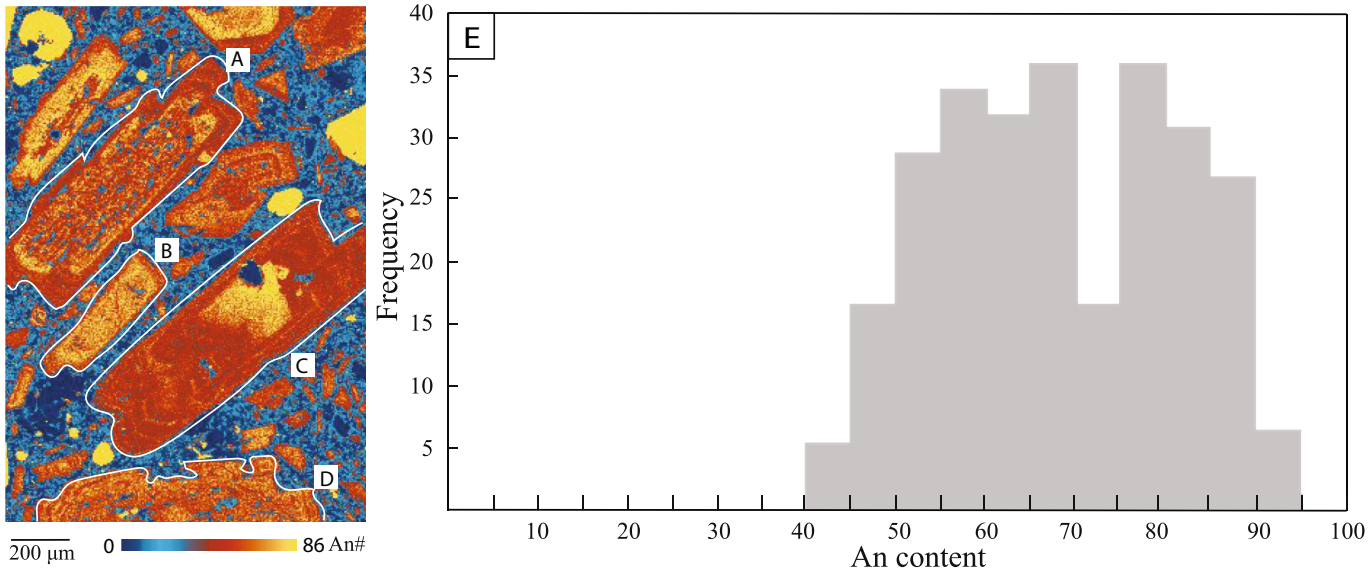


**Fig. 7.** Chemical map (this study) shows plagioclase data from sample TUR (cf. Fig. 1) showing (A) patchy, sieved low-An cores with high-An interfaces mantled by low-An plagioclase in equilibrium with the melt; (B) high-An cores overgrown by low-An mantles in equilibrium; (C) high-An cores with oscillatory zoned thick mantles; and (D) patchy zoned cores with no mantle and narrow rims. All crystal types occur within a short length scale of the order of 1 mm. (E) Histogram showing at least 2 populations of plagioclase with distinct An contents for all Taranaki crystals, built from a compilation of all plagioclase microprobe data published by D'Mello et al. (2023).

Clarke, 2010; Genareau et al., 2009; Giuffrida et al., 2018; Kent et al., 2007; Neukampf et al., 2021; Pontesilli et al., 2023). As a result, Li chemical disequilibium is often seen to increase from core to rims of plagioclase crystals, and this can be modelled through Li diffusion chronometry to constrain the timescales of those processes, typically yielding seconds to minutes at magmatic temperatures. The apparent lack of such disequilibria in most Taranaki plagioclase crystals suggests that neither degassing nor regassing processes have been recorded by the plagioclase crystal cargo. This may indicate that following crystal growth and long storage at depth, the crystal cargo has ascended rapidly in the final magma batch that breached the surface, too fast for significant degassing-induced crystal growth to occur (cf. Zellmer et al., 2024), and too fast for syn-eruptive Li diffusion to operate to an observable extent.

### 5.2.2. Clinopyroxene

*Inferences from Cr zoning.* Cr is highly compatible with clinopyroxene, and Cr enrichment coupled with depletion in incompatible elements indicates recharge with mafic magmas (Ubide and Kamber, 2018). However, the magmas of Taranaki are generally poor in Cr, indicating relatively felsic parental melts (D'Mello et al., 2023), and therefore Cr zoning in clinopyroxene is not a consistent recorder of magma recharge episodes at Taranaki. When detectable, Cr zoning shows either no variations, single or multiple enrichment zones in the mantle, an enriched core, or an enriched mantle (Fig. 8). These types of zoning patterns are indicative of heterogenous interaction of a mushy system with injected Cr rich melt, as suggested by Bergantz et al. (2017) and Ubide and Kamber (2018). It is possible that, during an intrusive event, some crystals never encountered the intruding melt and just experienced a thermal spike, while others had repeated interactions resulting in multiple zones of enrichment. This precludes the formation of an extensive, melt-rich mush zone and is more indicative of a plutonic basement that is intermittently intruded by melts to form pockets of mush that interact with only some of the crystals. The growth stage during which interaction occurs determines whether the enrichment is observed in the core, mantle, or the rim of the crystal. Another key observation is the difference in the concentration of Cr enrichment, varying from 300 to 5200 μg/g, which indicates different recharge episodes with variable concentrations of Cr, or variable mixing of recharge and resident melts, as e.g. observed at La Palma (Ubide et al., 2023). Taranaki lavas are relatively depleted in Cr with concentrations ranging from 25 to 45 μg/g except for two samples that show Cr contents of 120–145 μg/g. These enriched cores/zones may have formed due to the injection of slightly more primitive (but still relatively Cr-poor) melts. Alternatively, it is also possible that these crystals are xenocrysts formed during the crystallization of the Median Batholith or the early-stage Taranaki system and record injections of higher-Cr, mafic melts much before the formation of the present cone.

*Inferences from Na zoning.* Jadeite melting is sensitive to pressure changes, and higher Na in clinopyroxene cores is typically indicative of higher-pressure environments (Bédard, 2014; Blundy et al., 1995; Nimis, 1995). Experimental data suggest that changes in Na are primarily controlled by pressure, assuming the melt compositions are uniform. In turn, sector zoning only has weak influence on Na partitioning (MacDonald et al., 2023). In Taranaki clinopyroxenes, we see cores that have low Na content and are mantled by oscillatory zones. On a first assessment, this could suggest movement of crystals from a region of low pressure to high pressure. The history of the Taranaki volcano identifies phases of cone growth and collapse (Palmer and Neall, 1991; Procter et al., 2009; Zemeny et al., 2023; Zernack and Procter, 2021) that may have contributed to small changes in Na concentrations. However, given the diversity of melt compositions, it is more likely that the melt from which the cores crystallised was different in composition from the melt in which the mantles crystallised. It follows that clinopyroxene cores grew from more evolved melts than clinopyroxene mantles and rims, suggesting mafic recharge into evolved mushes or mushes grown from felsic primary melts rich in Na. The notion of variable primary melt compositions (D'Mello et al., 2023) is complemented by differences in the concentrations of other elements between core and mantle.

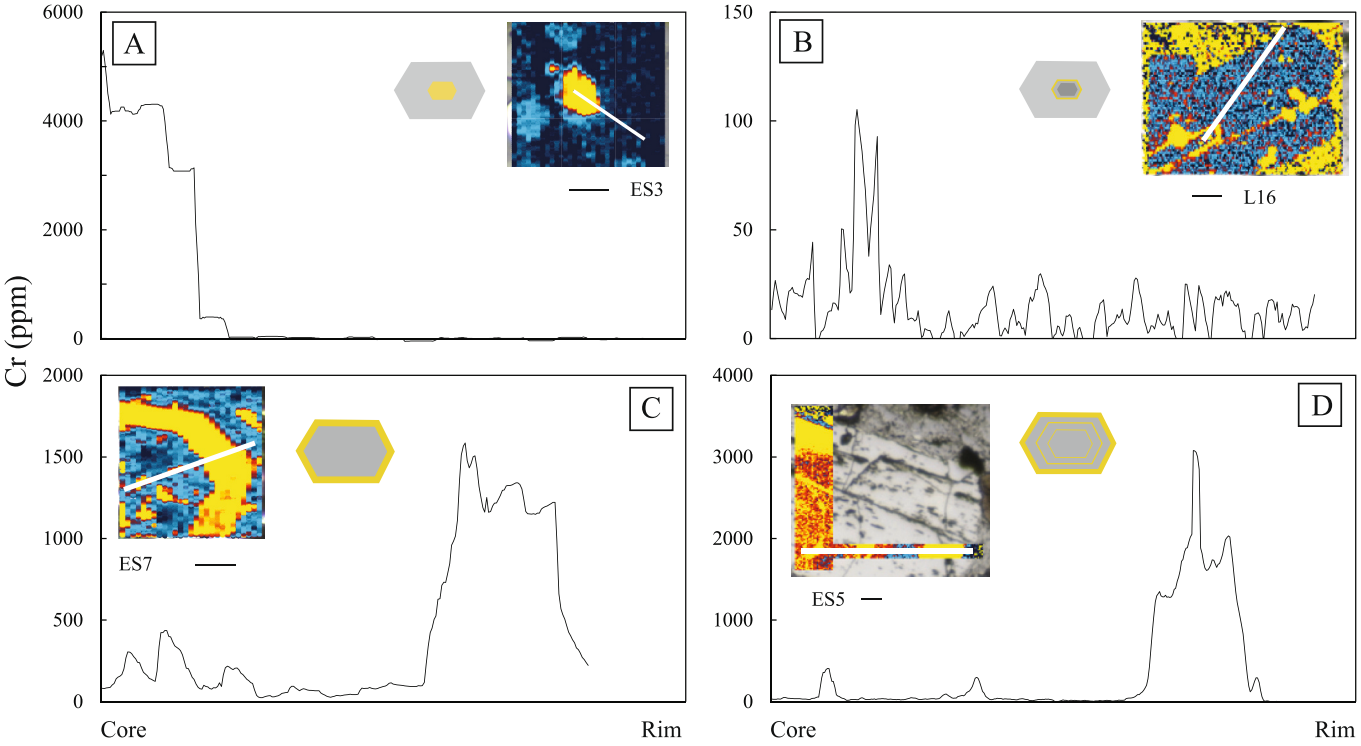


**Fig. 8.** Cr zonation patterns in clinopyroxene showing (A) low, flat Cr content from sample L5; (B) Cr enrichment marking resorption of the core in sample L16; (C) Cr-enriched rim in sample ES7; (D) multiple Cr enrichment episodes with high Cr enrichment in the rim in sample ES5. Refer to Fig. 1 for sample locations.

#### 5.2.3. Amphibole

*Inferences from Al zoning.* The composition of amphibole is affected by *P*, *T*, $fO_2$ and $P_{H_2O}$. Temperature increases cause an increase in Al, Na and Ti of amphibole (Scaillet and Evans, 1999). If the heating event is small enough, zones with increasing Al are formed, and if heating is substantial, magma temperatures beyond amphibole stability are attained, resulting in the formation of augite or the volumetric decomposition of amphibole. The latter is observed at Taranaki (D'Mello et al., 2021). The zoning of Al is preserved in amphibole macrocrysts and is rarely associated with an enrichment in Cr, indicating recharge events with high temperature melts of low Cr concentration.

*Inference from Mg zoning.* The Mg# of amphibole strongly increases with the increase in $fO_2$ of the system due to the decrease of $Fe^{2+}$ activity in the melt (Czamanske and Wones, 1973; Humphreys et al., 2006; Scaillet and Evans, 1999). Taranaki samples show the formation of Mg- and Si-rich rims, which are accompanied by a decrease in Ti, consistent with gradual cooling during crystallisation of the core (Bachmann and Dungan, 2002). Recharge events are also indicated by the sharp contacts between Mg-poor cores and Mg-rich rims.

### 5.3. Source of the Taranaki crystal cargo

The Taranaki volcanic system has been active for around 130,000 years (Zernack et al., 2011). Price et al. (2016) studied the xenoliths entrained in Taranaki lavas which provide unique insights into the crustal section beneath the volcano. Xenolith populations included: sedimentary material from the Taranaki Basin immediately beneath the volcano; plutonic rocks from the Median Batholith; and metamorphic rocks from the deeper crust. Xenoliths were divided into four types by Price et al. (2016): Types I-III are gabbroic and ultramafic xenoliths that differ with respect to the primary mineral phases present; while Type IV are rare peridotites. Based on the chemistry of the xenoliths, a magmatic reservoir characterized by mixing, assimilation, storage and hybridization (MASH) or a deep crustal hot zone (DCHZ) (Annen et al., 2006; Hildreth and Moorbath, 1988) had originally been proposed to have formed over time, trapping mantle-derived magmas that assimilated the wall rock and also fractionated (Price et al., 2016). However, D'Mello et al. (2023) recently questioned the existence of a DCHZ beneath Taranaki on basis of new mineral-melt geothermometric and hygrometric constraints: temperatures are too high and compositions are not hydrous enough to be consistent with DCHZ differentiation processes of the intermediate Taranaki magma compositions.

The wall rocks can be correlated to the Median Tectonic Zone (MTZ), defined as a zone of deformed or dismembered small crustal fragments and/or magmatic arc rocks (Bradshaw, 1993; Frost and Coombs, 1989; Kimbrough et al., 1994). It includes terranes, formations, plutons, igneous complexes and gneisses (Mortimer et al., 1999b). This zone also forms the basement for the Taranaki Peninsula overlain by the sediments of the Taranaki Basin (Mortimer et al., 1997). The MTZ plutons are of Carboniferous to early Cretaceous age and are mainly of calc-alkaline I-type petrological character (Kimbrough et al., 1994). The Median Batholith is defined as a large volume composite intrusion comprising many individual but contiguous plutonic and metaplutonic rocks (Mortimer et al., 1999a). It represents the main locus of magmatism in the New Zealand sector of Gondwana and probably developed *in situ* as a result of the interaction of the Panthalassan oceanic plates with the South Gondwana continental plate (Mortimer et al., 1999b). While the diversity of bulk rock composition within the Median Batholith, which spans the entire length of New Zealand, is clear, there is no exposure of these rocks in the Taranaki region, and there are no microanalytical or mineral textural data available for any of these rocks to our knowledge.

The Taranaki volcanic system is much younger than the 120 Myr Median Batholith. However, the similar magmatic origin of the two systems leads to the question as to whether the minerals present in the Taranaki lavas crystallized during the earlier stages of the Taranaki system (antecrystic) or whether they are derived from the older, Median Batholith magmatic system (xenocrystic). D'Mello et al. (2023) showed that in terms of major oxide compositions, the phenocrysts of Taranaki compositionally fully overlap with the crystals from the Taranaki xenoliths studied previously (Gruender et al., 2010; Price et al., 2016). Further, certain petrological textures, such as sieve, cellular and oscillatory zoning of plagioclase and the sieve and sector zoning of clinopyroxene require repeated injections of mafic intrusions and low degrees of undercooling. While such textures may be explained by dynamic magmatic processes in large thermally buffered mushy reservoirs, they are also consistent with crystallisation in small and rapidly cooling mush pockets solidifying into plutonic bodies in an overall colder crustal environment. We prefer the latter interpretation, because it is more consistent with the vast diversity of textures found within individual samples (e.g., Fig. 7A-D) in conjunction with the compositional overlap of phenocrysts with crystals of the plutonic xenoliths sourced from a subsolidus crustal environment.

We hypothesise that at the Taranaki Volcanic Lineament, crystallization of repeated intrusions of mantle derived melts over a long period of time have developed an extensive plutonic system in the crust, which may be repeatedly re-intruded to form small pockets of supersolidus crystal mush. The bulk of the crystal populations in these mush pockets are crystal clots and disengaged crystals that have interacted with the injected interstitial melt of varying compositions and volumes. This includes large clots of amphibole, clinopyroxene, and plagioclase, which are taken to represent disintegrating plutonic xenoliths (cf. Zellmer et al., 2024), thereby inheriting the magmatic signatures of the plutonic rocks sourced from the up to at least 130 kyr older Taranaki system and potentially the *c.* 120 Myr old Median Batholith. Subsequent evolution of the plutonic system and continued intrusion of subduction derived melts from the current east New Zealand system feeds the present edifice of Mt. Taranaki. The longevity of this system and the complexities of the tectonic context and melt generation have yielded a crystal cargo that reflects these complex magmatic processes, including remobilization of heterogeneous mafic plutonic rocks generated in the earlier phases of Taranaki magmatism and possibly the much older generation of the Median batholith that formed >100 million years ago.

### 5.4. Petrogenesis of Taranaki lavas

Lavas erupted from Taranaki show varying compositions and mineral assemblages ranging from basalts to dacites. Whole rock compositions can be interpreted as the sum product of diverse melt compositions and uptake of crystals in varying proportions (cf. D'Mello et al., 2023) from plutonic precursors, which have then reacted with the melt to varying degrees during storage in mush pockets.

The magnitude of recharge events can be assessed from ubiquitous textures such as sieved plagioclase macrocrysts and reacted amphiboles. Plagioclase macrocrysts with sieve textures suggest that either (i) a large volume of freshly injected magma interacted with all crystals in a mush zone, or (ii) that the sieve texture is much older and is a feature that is preserved from when the crystal initially formed. Reacted amphiboles, on the other hand, are indicative of a late-stage process (during ascent) where all crystals are subject to decompression during ascent (D'Mello et al., 2021). On the other hand, comparatively small volume events do not significantly change the bulk properties of mushy reservoirs and are reflected in the limited proportions of crystals that show such changes in conditions. Small volume events facilitate the contemporaneous growth of different zoning types in different parts of the storage zone. For macrocrysts with different zoning patterns to erupt in the same sample, melt homogenization and mixing must happen only shortly before eruption.

The presence of glomerocrysts with intergrown clinopyroxene, clinopyroxene + plagioclase, magnetite and amphibole indicate a crystal rich environment with crystal faces impeding on the growth of other crystals (Holness et al., 2019; Holness et al., 2007b). These textures are common in xenoliths found in Taranaki lavas and debris avalanche

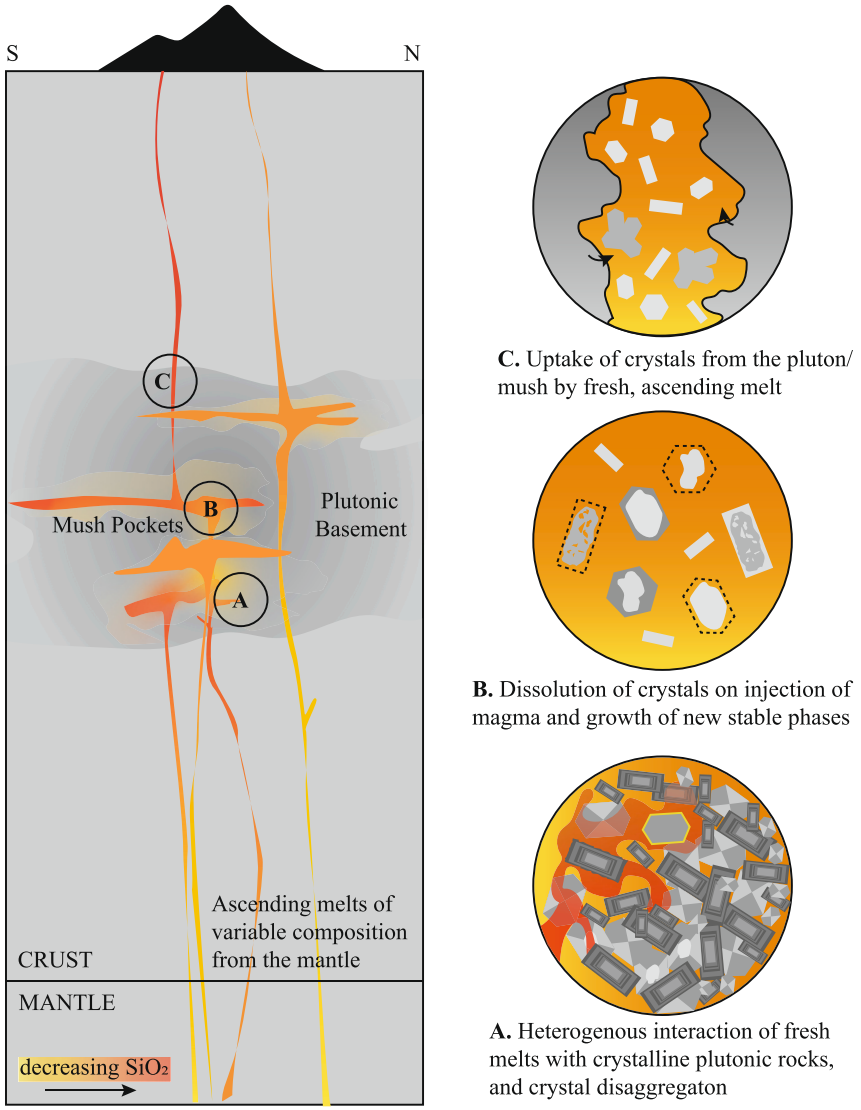


**Fig. 9.** Model for Taranaki eruptives. (A) Melts with variable compositions (low- to high-$SiO_2$) from the mantle pick up crystals and crystal clots from the country rock (Median Batholith) resulting in a population of xenocrystic crystals within an otherwise aphyric to sparsely phyric melt. (B) during storage within the mush zone, these xenocrystic/antecrystic cores are then resorbed or dissolved, followed by euhedral overgrowth of new material on remnant crystal cores. (C) Influxes of fresh melts of varying compositions interact heterogeneously with the subvolcanic basement, affecting crystal compositions and zoning patterns provided the crystal come in contact with the melt. Vertical scale purposefully omitted as pressures, besides being crustal, are largely unconstrained (D'Mello et al., 2023).

deposits and are expected from fragments of rigid crystal sponges or solid plutonic precursor rocks. These plutonic rocks, when intruded by melts, disaggregate to form glomerocrysts entrained in the fresh magmas, and glomerocrysts may disaggregate further to form antecrysts or xenocrysts (Zellmer et al., 2024).

Thus, magma intrusions may disaggregate parts of these plutonic protoliths into small and ephemeral crystal-rich mush pockets. Glomerocryst disaggregation results in free crystals, experiencing different sequences of processes, which include mixing, ascent, and remobilization. Transport of crystals and recrystallization results in a euhedral outline of the clinopyroxene macrocrysts. The texture and composition of these crystals respond not only to thermodynamic conditions, but also to kinetic effects during crystal growth; for example, variable degrees of undercooling or rapid decompression (Lofgren et al., 2006; MacDonald et al., 2023; Masotta et al., 2020; Mollo et al., 2013; Mollo et al., 2010; Neave et al., 2019; Pontesilli et al., 2019).

The disparities in zoning patterns found in crystals of the same lava flow indicate that these crystals must have grown apart, before mixing and melt homogenization were complete as reflected by crystals with rims with comparable compositions to groundmass microlites that formed from the carrier melt. This is accomplished through a final recharge episode, which picks up crystals with varying growth and storage histories, and the crystal-melt mixture ultimately ascends rapidly through the plumbing system to breach the surface at eruption.

Fig. 9 illustrates the plumbing system of Mt. Taranaki envisaged here. Ascending melts interact with the plutonic basement forming local mush pockets within the plutonic system. Initial interaction results in the dislodging and disintegration of plutonic protoliths into crystal clots within a mush pocket formed due to remobilization by recharging melts (Fig. 9A). These crystals and glomerocrysts begin to interact with the melt through resorption and regrowth of crystals resulting in anhedral cores with euhedral-subhedral mantles and rims (Fig. 9B). Over time, the plutonic system evolves, and each new injection of melt interacts with and remobilizes crystals from different storage regions, resulting in a highly heterogeneous crystalline basement (Fig. 9C). During larger injections of melts that trigger eruptions, crystals are remobilized from these different parts of the subvolcanic storage environment and ascend to the surface, thus resulting in crystals with different thermal and

growth histories found over short lengths of a few millimetres within the erupted lava flow deposits.

## 6. Conclusions

1. The lava flows of Taranaki volcano have a rich crystal cargo with diverse chemical zoning patterns and textures, suggesting varied sequences of magmatic processes recorded in the crystals. These processes include magma recharge, remobilization of solid precursor rocks, and interaction of crystal cargo with mafic as well as felsic melts.
2. The crystalline basement of Taranaki is a product of repeated injections of melts from subduction systems that formed the *c*. 120 Myr old Median Batholith as well as consanguineous plutons of the more recent magmatic system active over the last 130 kyr. These subsolidus plutonic rocks disengage crystal clots that subsequently undergo dissolution and overgrowth crystallisation.
3. The subvolcanic basement is highly heterogenous, and the extent and influence of each new intrusion is largely dependent on its volume. Small volume intrusions result in different sub-environments (mush pockets) with unique compositions and intrinsic parameters.
4. The final magmatic pulse that ultimately results in an eruption remobilises crystals from different environments, triggering crystallization of microlites and rims on the heterogenous crystal cargo prior to extrusion.

## CRediT authorship contribution statement

**Nessa G. D'Mello:** Writing – original draft, Visualization, Validation, Software, Resources, Methodology, Investigation, Formal analysis, Data curation. **Georg F. Zellmer:** Writing – review & editing, Validation, Supervision, Software, Resources, Project administration, Investigation, Funding acquisition, Formal analysis, Data curation, Conceptualization. **Teresa Ubide:** Writing – review & editing, Validation, Supervision, Software, Resources, Methodology, Investigation, Funding acquisition, Formal analysis. **John Caulfield:** Validation, Supervision, Software, Methodology, Investigation. **Masako Usuki:** Supervision, Software, Resources, Methodology, Investigation. **Yoshiyuki Iizuka:** Validation, Supervision, Software, Resources, Methodology, Investigation. **Gabor Kereszturi:** Writing – review & editing, Supervision. **Jon N. Procter:** Supervision. **Robert B. Stewart:** Resources.

## Declaration of competing interest

Teresa Ubide reports financial support was provided by Australian Research Council. If there are other authors, they declare that they have no known competing financial interests or personal relationships that could have appeared to influence the work reported in this paper.

## Data availability

All new data published in this article is available within the article and its supplementary materials.

## Acknowledgments

The lead author acknowledges a Massey Foundation Scholarship to visit the University of Queensland for the chemical mapping of trace elements in the crystal cargo studied here, and a School of Agriculture and Environment stipend during the period of data collection. TU was supported by an Australian Research Council Future Fellowship (ARC FT230100230). We thank Silvio Mollo and an anonymous reviewer for constructive comments that improved an earlier version of this paper, and Claudia Romano for editorial handling.

## Appendix A. Supplementary data

Supplementary data to this article can be found online at https://doi.org/10.1016/j.chemgeo.2024.122333.

## References

Alloway, B., et al., 2005a. Stratigraphy, age, and correlation of voluminous debris-avalanche events from an ancestral Egmont Volcano: implications for coastal plain construction and regional hazard assessment. J. R. Soc. N. Z. 35 (1–2), 229–267.
Alloway, B.V., Pillans, B.J., Carter, L., Naish, T.R., Westgate, J.A., 2005b. Onshore-offshore correlation of Pleistocene rhyolitic eruptions from New Zealand: implications for TVZ eruptive history and paleoenvironmental construction. Quat. Sci. Rev. 24 (14–15), 1601–1622.
Almeev, R.R., Holtz, F., Koepke, J., Parat, F., 2012. Experimental calibration of the effect of H2O on plagioclase crystallization in basaltic melt at 200 MPa. Am. Mineral. 97 (7), 1234–1240.
Annen, C., Blundy, J.D., Sparks, R.S.J., 2006. The genesis of intermediate and silicic magmas in deep crustal hot zones. J. Petrol. 47 (3), 505–539.
Bachmann, O., Bergantz, G.W., 2008. Rhyolites and their source mushes across tectonic settings. J. Petrol. 49 (12), 2277–2285.
Bachmann, O., Dungan, M.A., 2002. Temperature-induced Al-zoning in hornblendes of the Fish Canyon magma, Colorado. Am. Miner. 87 (8–9), 1062–1076.
Bédard, J.H., 2014. Parameterizations of calcic clinopyroxene - Melt trace element partition coefficients. Geochem. Geophys. Geosyst. 15 (2), 303–336.
Bennett, E.N., Lissenberg, C.J., Cashman, K.V., 2019. The significance of plagioclase textures in mid-ocean ridge basalt (Gakkel Ridge, Arctic Ocean). Contrib. Mineral. Petrol. 174 (6).
Bergantz, G.W., Schleicher, J.M., Burgisser, A., 2017. On the kinematics and dynamics of crystal-rich systems. J. Geophys. Res. Solid Earth 122 (8), 6131–6159.
Berlo, K., Turner, S., Blundy, J., Hawkesworth, C., 2004. The extent of U-series disequilibria produced during partial melting of the lower crust with implications for the formation of the Mount St. Helens dacites. Contrib. Mineral. Petrol. 148 (1), 122–130.
Bindeman, I.N., Davis, A.M., 2000. Trace element partitioning between plagioclase and melt: investigation of dopant influence on partition behavior. Geochim. Cosmochim. Acta 64 (16), 2863–2878.
Bindeman, I.N., Davis, A.M., Drake, M.J., 1998. Ion microprobe study of plagioclase-basalt partition experiments at natural concentration levels of trace elements. Geochim. Cosmochim. Acta 62 (7), 1175–1193.
Blundy, J.D., Wood, B.J., 1991. Crystal-chemical controls on the partitioning of Sr and Ba between plagioclase feldspar, silicate melts, and hydrothermal solutions. Geochim. Cosmochim. Acta 55 (1), 193–209.
Blundy, J.D., Falloon, T.J., Wood, B.J., Dalton, J.A., 1995. Sodium partitioning between clinopyroxene and silicate melts. J. Geophys. Res. 100 (B8), 15,501–15,515.
Blundy, J., Cashman, K.V., Berlo, K., 2008. Evolving magma storage conditions beneath Mount St. Helens inferred from chemical variations in melt inclusions from the 1980–1986 and current (2004–2006) eruptions. US Geol. Surv. Prof. Pap. (1750), 755–790.
Bowen, N.L., 1913. The melting phenomena of the plagioclase feldspars. Am. J. Sci. 35 (210), 577–599.
Bradshaw, J., 1993. A review of the Median Tectonic Zone: terrane boundaries and terrane amalgamation near the Median Tectonic Line. N. Z. J. Geol. Geophys. 36 (1), 117–125.
Cashman, K.V., Sparks, R.S.J., Blundy, J.D., 2017. Vertically extensive and unstable magmatic systems: A unified view of igneous processes. Science 355, eaag3055.
Charlier, B., et al., 2012. Lithium concentration gradients in feldspar and quartz record the final minutes of magma ascent in an explosive supereruption. Earth Planet. Sci. Lett. 319, 218–227.
Cherniak, D.J., 2010. Cation diffusion in feldspars. Rev. Mineral. Geochem. 72, 691–733.
Colle, F., et al., 2023. Effect of undercooling on clinopyroxene crystallization in a high K basalt: Implications for magma dynamics at Stromboli volcano. Lithos 456–457, 107327.
Coogan, L.A., 2011. Preliminary experimental determination of the partitioning of lithium between plagioclase crystals of different anorthite contents. Lithos 125 (1–2), 711–715.
Coogan, L.A., Saunders, A.D., Kempton, P.D., Norry, M.J., 2000. Evidence from oceanic gabbros for porous melt migration within a crystal mush beneath the Mid-Atlantic Ridge. Geochem. Geophys. Geosyst. 1 (9).
Costa, F., Andreastuti, S., Bouvet de Maisonneuve, C., Pallister, J.S., 2013. Petrological insights into the storage conditions, and magmatic processes that yielded the centennial 2010 Merapi explosive eruption. J. Volcanol. Geotherm. Res. 261, 209–235.
Coulthard Jr., D.A., et al., 2024. Plutonic nature of a transcrustal magmatic system: evidence from ultrahigh resolution Sr-disequilibria in plagioclase microantecrysts from the southern Taupo Volcanic Zone, New Zealand. J. Petrol. 65, egad087.
Czamanske, G.K., Wones, D.R., 1973. Oxidation during magmatic differentiation, Finnmarka complex, Oslo Area, Norway: Part 2, the mafic silicates1. J. Petrol. 14 (3), 349–380.
Damaschke, M., Cronin, S.J., Holt, K.A., Bebbington, M.S., Hogg, A.G., 2017. A 30,000 yr high-precision eruption history for the andesitic Mt. Taranaki, North Island, New Zealand. Quaternary Research (United States) 87 (1), 1–23.
de Maisonneuve, C.B., et al., 2016. How do olivines record magmatic events? Insights from major and trace element zoning. Contrib. Mineral. Petrol. 171 (6).

Degruyter, W., Huber, C., Bachmann, O., Cooper, K.M., Kent, A.J.R., 2016. Magma reservoir response to transient recharge events: The case of Santorini volcano (Greece). Geology 44 (1), 23–26.
D'Mello, N.G., et al., 2021. Deciphering magma storage and ascent processes of Taranaki, New Zealand, from the complexity of amphibole breakdown textures. Lithos 106264.
D'Mello, N.G., et al., 2023. Crystal entrainment from cool, low-silica rocks into hot, high-silica melts: diverse primary melt compositions at Taranaki volcano, New Zealand. J. Geol. Soc. 180 jgs2022–036.
Downes, M.J., 1974. Sector and oscillatory zoning in calcic augites from M. Etna, Sicily. Contrib. Mineral. Petrol. 47 (3), 187–196.
Drake, M.J., 1976. Plagioclase-melt equilibria. Geochim. Cosmochim. Acta 40 (4), 457–465.
Elardo, S.M., Shearer, C.K., 2014. Magma chamber dynamics recorded by oscillatory zoning in pyroxene and olivine phenocrysts in basaltic lunar meteorite Northwest Africa 032. Am. Mineral. 99 (2–3), 355–368.
Ellis, B.S., et al., 2018. Post-eruptive mobility of lithium in volcanic rocks. Nat. Commun. 9 (1), 3228.
Frost, C., Coombs, D., 1989. Nd isotope character of New Zealand sediments; implications for terrane concepts and crustal evolution. Am. J. Sci. 289 (6), 744–770.
Ganne, J., Bachmann, O., Feng, X., 2018. Deep into magma plumbing systems: Interrogating the crystal cargo of volcanic deposits. Geology 46 (5), 415–418.
Genareau, K., Clarke, A.B., 2010. In situ measurements of plagioclase growth using SIMS depth profiles of 7Li/30Si: A means to acquire crystallization rates during short-duration decompression events. Am. Mineral. 95 (4), 592–601.
Genareau, K., Clarke, A.B., Hervig, R.L., 2009. New insight into explosive volcanic eruptions: Connecting crystal-scale chemical changes with conduit-scale dynamics. Geology 37 (4), 367–370.
Giletti, B.J., Casserly, J.E.D., 1994. Strontium diffusion kinetics in plagioclase feldspars. Geochim. Cosmochim. Acta 58 (18), 3785–3793.
Giletti, B.J., Shanahan, T.M., 1997. Alkali diffusion in plagioclase feldspar. Chem. Geol. 139 (1–4), 3–20.
Ginibre, C., Wörner, G., 2007. Variable parent magmas and recharge regimes of the Parinacota magma system (N. Chile) revealed by Fe, Mg and Sr zoning in plagioclase. Lithos 98 (1–4), 118–140.
Ginibre, C., Kronz, A., Wörner, G., 2002a. High-resolution quantitative imaging of plagioclase composition using accumulated backscattered electron images: New constraints on oscillatory zoning. Contrib. Mineral. Petrol. 142 (4), 436–448.
Ginibre, C., Wörner, G., Kronz, A., 2002b. Minor- and trace-element zoning in plagioclase: Implications for magma chamber processes at Parinacota volcano, northern Chile. Contrib. Mineral. Petrol. 143 (3), 300–315.
Ginibre, C., Wörner, G., Kronz, A., 2007. Crystal zoning as an archive for magma evolution. Elements 3 (4), 261–266.
Giuffrida, M., Viccaro, M., Ottolini, L., 2018. Ultrafast syn-eruptive degassing and ascent trigger high-energy basic eruptions. Sci. Rep. 8 (1), 1–7.
Grove, T.L., Kinzler, R.J., Bryan, W.B., 1992. Fractionation of mid-ocean ridge basalt (MORB). In: Mantle Flow and Melt Generation at Mid-Ocean Ridges, 71, pp. 281–310.
Gruender, K., Stewart, R.B., Foley, S., 2010. Xenoliths from the sub-volcanic lithosphere of Mt Taranaki, New Zealand. J. Volcanol. Geotherm. Res. 190 (1–2), 192–202.
Hawthorne, F.C., et al., 2012. Nomenclature of the amphibole supergroup. Am. Mineral. 97 (11–12), 2031–2048.
Hildreth, W., 2004. Volcanological perspectives on Long Valley, Mammoth Mountain, and Mono Craters: several contiguous but discrete systems. J. Volcanol. Geotherm. Res. 136 (3), 169–198.
Hildreth, W., Moorbath, S., 1988. Crustal contributions to arc magmatism in the Andes of Central Chile. Contrib. Mineral. Petrol. 98 (4), 455–489.
Hollister, L.S., Gancarz, A.J., 1971. Compositional sector-zoning in clinopyroxene from the Narce area, Italy. Am. Mineral. 56 (5–6), 959–979.
Holness, M.B., et al., 2007a. Textures in partially solidified crystalline nodules: A window into the pore structure of slowly cooled mafic intrusions. J. Petrol. 48 (7), 1243–1264.
Holness, M.B., Tegner, C., Nielsen, T.F.D., Stripp, G., Morse, S.A., 2007b. A textural record of solidification and cooling in the skaergaard intrusion, East Greenland. J. Petrol. 48 (12), 2359–2377.
Holness, M.B., Stock, M.J., Geist, D., 2019. Magma chambers versus mush zones: Constraining the architecture of sub-volcanic plumbing systems from microstructural analysis of crystalline enclaves. Philos. Trans. R. Soc. A Math. Phys. Eng. Sci. 377 (2139).
Humphreys, M.C.S., Blundy, J.D., Sparks, R.S.J., 2006. Magma evolution and open-system processes at Shiveluch Volcano: Insights from phenocryst zoning. J. Petrol. 47 (12), 2303–2334.
Iddings, J.P., 1892. On the crystallization of igneous rocks. In: Bulletin of the Philosophical Society of Washington, XI, pp. 71–112.
Johannes, W., Koepke, J., Behrens, H., 1994. Partial melting reactions of plagioclases and plagioclase-bearing systems. Feldspars and Their Reactions 161–194.
Kahl, M., Chakraborty, S., Costa, F., Pompilio, M., 2011. Dynamic plumbing system beneath volcanoes revealed by kinetic modeling, and the connection to monitoring data: An example from Mt. Etna. Earth and Planetary Science Letters 308 (1–2), 11–22.
Kahl, M., Viccaro, M., Ubide, T., Morgan, D.J., Dingwell, D.B., 2017. A branched magma feeder system during the 1669 eruption of Mt Etna: Evidence from a time-integrated study of zoned olivine phenocryst populations. J. Petrol. 58 (3), 443–472.
Kent, A.J., et al., 2007. Vapor transfer prior to the October 2004 eruption of Mount St. Helens, Washington. Geology 35 (3), 231–234.
Kimbrough, D., et al., 1994. Uranium-lead zircon ages from the median tectonic zone, New Zealand. N. Z. J. Geol. Geophys. 37 (4), 393–419.
Lange, A.E., Nielsen, R.L., Tepley, F.J., Kent, A.J.R., 2013. The petrogenesis of plagioclase-phyric basalts at mid-ocean ridges. Geochem. Geophys. Geosyst. 14 (8), 3282–3296.
Lerner, G.A., Cronin, S.J., Bebbington, M.S., Platz, T., 2019. The characteristics of a multi-episode volcanic regime: the post-AD 960 Maero Eruptive Period of Mt. Taranaki (New Zealand). Bull. Volcanol. 81 (11), 1–24.
Leung, I.S., 1974. Sector-zoned titanaugites: Morphology, crystal chemistry, and growth. Am. Mineral. 59 (1–2), 127–138.
Lissenberg, C.J., MacLeod, C.J., 2016. A reactive porous flow control on mid-ocean ridge magmatic evolution. J. Petrol. 57 (11–12), 2195–2220.
Lofgren, G.E., Huss, G.R., Wasserburg, G.J., 2006. An experimental study of trace-element partitioning between Ti-Al-clinopyroxene and melt: Equilibrium and kinetic effects including sector zoning. Am. Mineral. 91 (10), 1596–1606.
Longhi, J., Fram, M.S., Vander Auwera, J., Montieth, J.N., 1993. Pressure effects, kinetics, and rheology of anorthositic and related magmas. Am. Mineral. 78, 1016–1030.
MacDonald, A., Ubide, T., Mollo, S., Masotta, M., Pontesilli, A., 2022. Trace element partitioning in zoned clinopyroxene as a proxy for undercooling: Experimental constraints from trachybasaltic magmas. Geochim. Cosmochim. Acta 336, 249–268.
MacDonald, A., Ubide, T., Mollo, S., Pontesilli, A., Masotta, M., 2023. The influence of undercooling and sector zoning on clinopyroxene–melt equilibrium and thermobarometry. J. Petrol. 64 (10).
MacDonald, A., Ubide, T., Mollo, S., 2024. Degree of sector zoning in clinopyroxene records dynamic magma recharge and ascent. Geochim. Cosmochim. Acta 378, 245–258.
Masotta, M., et al., 2020. The role of undercooling during clinopyroxene growth in trachybasaltic magmas: Insights on magma decompression and cooling at Mt. Etna volcano. Geochimica et Cosmochimica Acta 268, 258–276.
Mollo, S., Del Gaudio, P., Ventura, G., Iezzi, G., Scarlato, P., 2010. Dependence of clinopyroxene composition on cooling rate in basaltic magmas: Implications for thermobarometry. Lithos 118 (3–4), 302–312.
Mollo, S., Blundy, J.D., Iezzi, G., Scarlato, P., Langone, A., 2013. The partitioning of trace elements between clinopyroxene and trachybasaltic melt during rapid cooling and crystal growth. Contrib. Mineral. Petrol. 166 (6), 1633–1654.
Mollo, S., et al., 2015. Reconstruction of magmatic variables governing recent Etnean eruptions: Constraints from mineral chemistry and P-T-fO2-H2O modeling. Lithos 212–215, 311–320.
Mollo, S., Ubide, T., Di Stefano, F., Nazzari, M., Scarlato, P., 2020. Polybaric/polythermal magma transport and trace element partitioning recorded in single crystals: A case study of a zoned clinopyroxene from Mt. Etna. Lithos 356–357.
Morimoto, M., 1988. Nomenclature of pyroxenes. Mineral. Mag. 52 (4), 535–550.
Mortimer, N., Tulloch, A.J., Ireland, T.R., 1997. Basement geology of Taranaki and Wanganui Basins, New Zealand. N. Z. J. Geol. Geophys. 40 (2), 223–236.
Mortimer, N., Gans, P., Calvert, A., Walker, N., 1999a. Geology and thermochronometry of the east edge of the Median Batholith (Median Tectonic Zone): A new perspective on Permian to Cretaceous crustal growth of New Zealand. Island Arc 8 (3), 404–425.
Mortimer, N., et al., 1999b. Overview of the Median Batholith, New Zealand: A new interpretation of the geology of the Median Tectonic Zone and adjacent rocks. J. Afr. Earth Sci. 29 (1), 257–268.
Moschini, P., et al., 2023. A review of plagioclase growth rate and compositional evolution in mafic alkaline magmas: Guidelines for thermometry, hygrometry, and timescales of magma dynamics at Stromboli and Mt. Etna. Earth-Science Reviews 240, 104399.
Nakamura, M., 1995. Residence time and crystallization history of nickeliferous olivine phenocrysts from the northern Yatsugatake volcanoes, Central Japan: Application of a growth and diffusion model in the system Mg-Fe-Ni. J. Volcanol. Geotherm. Res. 66 (1–4), 81–100.
Nakamura, M., Shimakita, S., 1998. Dissolution origin and syn-entrapment compositional change of melt inclusion in plagioclase. Earth Planet. Sci. Lett. 161 (1–4), 119–133.
Namur, O., Charlier, B., Toplis, M.J., Vander Auwera, J., 2012. Prediction of plagioclase-melt equilibria in anhydrous silicate melts at 1-atm. Contrib. Mineral. Petrol. 163 (1), 133–150.
Neall, V.E., Stewart, R.B., Smith, I.E.M., 1986. History and petrology of the Taranaki volcanoes. Late Cenozoic volcanism in New Zealand 23, 251–263.
Neave, D.A., Maclennan, J., 2020. Clinopyroxene Dissolution Records Rapid Magma Ascent. Front. Earth Sci. 8, 188.
Neave, D.A., et al., 2019. Clinopyroxene-Liquid Equilibria and Geothermobarometry in Natural and Experimental Tholeiites: The 2014–2015 Holuhraun Eruption, Iceland. Journal of Petrology 60 (8), 1653–1680.
Nelson, S.T., Montana, A., 1992. Sieve-textured plagioclase in volcanic rocks produced by rapid decompression. Am. Mineral. 77 (11–12), 1242–1249.
Neukampf, J., et al., 2021. Time scales of syneruptive volatile loss in silicic magmas quantified by Li isotopes. Geology 49 (2), 125–129.
Nicotra, E., Viccaro, M., 2012. Unusual magma storage conditions at Mt. Etna (Southern Italy) as evidenced by plagioclase megacryst-bearing lavas: Implications for the plumbing system geometry and summit caldera collapse. Bull. Volcanol. 74 (4), 795–815.
Nielsen, R.L., Ustunisik, G., Lange, A.E., Tepley, F.J., Kent, A.J.R., 2020. Trace Element and Isotopic Characteristics of Plagioclase Megacrysts in Plagioclase Ultraphyric Basalts (PUB). Geochem. Geophys. Geosyst. 21 (2).
Nimis, P., 1995. A clinopyroxene geobarometer for basaltic systems based on crystal-structure modeling. Contrib. Mineral. Petrol. 121 (2), 115–125.
O'Brien, H.E., Irving, A.J., McCallum, I.S., 1988. Complex zoning and resorption of phenocrysts in mixed potassic mafic magmas of the Highwood Mountains, Montana. Am. Mineral. 73, 1007–1024.

Palmer, B.A., Neall, V.E., 1991. Contrasting lithofacies architecture in ring-plain deposits related to edifice construction and destruction, the Quaternary Stratford and Opunake Formations, Egmont Volcano, New Zealand. Sedimentary Geology 74 (1), 71–88.
Pan, S., et al., 2018. Spongy texture in mantle clinopyroxene records decompression-induced melting. Lithos 320–321, 144–154.
Platz, T., 2007. Aspects of Dome-forming Eruptions from Andesitic Volcanoes through the Maero Eruptive Period (1000 yrs BP to Present) Activity at Mt. Taranaki.
Platz, T., Cronin, S.J., Cashman, K.V., Stewart, R.B., Smith, I.E.M., 2006. Transition from effusive to explosive phases in andesite eruptions - A case-study from the AD1655 eruption of Mt. Taranaki, New Zealand. J. Volcanol. Geotherm. Res. 161 (1–2), 15–34.
Pontesilli, A., et al., 2019. Crystallization kinetics of clinopyroxene and titanomagnetite growing from a trachybasaltic melt: New insights from isothermal time-series experiments. Chem. Geol. 510, 113–129.
Pontesilli, A., et al., 2023. The efficacy of high frequency petrological investigation at open-conduit volcanoes: The case of May 11 2019 explosions at southwestern and northeastern craters of Stromboli. Lithos 454–455, 107255.
Price, R.C., et al., 2016. High-K andesite petrogenesis and crustal evolution: Evidence from mafic and ultramafic xenoliths, Egmont Volcano (Mt. Taranaki) and comparisons with Ruapehu Volcano, North Island. New Zealand. Geochimica et Cosmochimica Acta 185, 328–357.
Price, R., Cronin, S., Smith, I., Ukstins, I., Zernack, A., 2021. Formation of crystal-rich, mixed, intermediate lavas at Pouakai Volcano and the evolution of the Taranaki volcanic lineament, western North Island, New Zealand. Lithos 380, 105850.
Procter, J.N., Cronin, S.J., Zernack, A.V., 2009. Landscape and sedimentary response to catastrophic debris avalanches, western Taranaki, New Zealand. Sedimentary Geology 220 (3–4), 271–287.
Putirka, K.D., 2008. Thermometers and barometers for volcanic systems. Rev. Mineral. Geochem. 61–120.
Putirka, K., Johnson, M., Kinzler, R., Longhi, J., Walker, D., 1996. Thermobarometry of mafic igneous rocks based on clinopyroxene-liquid equilibria, 0–30 kbar. Contrib. Mineral. Petrol. 123 (1), 92–108.
Scaillet, B., Evans, B.W., 1999. The 15 June 1991 eruption of Mount Pinatubo. I. Phase equilibria and pre-eruption P-T-fO2-fH2O conditions of the dacite magma. J. Petrol. 40 (3), 381–411.
Schoneveld, L., et al., 2020. Zoned Pyroxenes as prospectivity indicators for magmatic Ni-Cu sulfide mineralization. Front. Earth Sci. 8, 256.
Schwandt, C.S., McKay, G.A., 2006. Minor- and trace-element sector zoning in synthetic enstatite. Am. Mineral. 91 (10), 1607–1615.
Sherburn, S., White, R.S., 2005. Crustal seismicity in Taranaki, New Zealand using accurate hypocentres from a dense network. Geophys. J. Int. 162 (2), 494–506.
Shore, M., Fowler, A.D., 1996. Oscillatory zoning in minerals: A common phenomenon. Can. Mineral. 34 (6), 1111–1126.
Sparks, R.S.J., et al., 2019. Formation and dynamics of magma reservoirs. Philos. Trans. R. Soc. A Math. Phys. Eng. Sci. 377 (2139).
Stewart, M.L., Pearce, T.H., 2004. Sieve-textured plagioclase in dacitic magma: Interference imaging results. Am. Mineral. 89 (2–3), 348–351.
Streck, M.J., 2008. Mineral textures and zoning as evidence for open system processes. Rev. Mineral. Geochem. 595–622.
Streck, M.J., Leeman, W.P., Chesley, J., 2007. High-magnesian andesite from Mount Shasta: A product of magma mixing and contamination, not a primitive mantle melt. Geology 35, 351–354.
Tomiya, A., Takahashi, E., 2005. Evolution of the magma chamber beneath Usu Volcano since 1663: a natural laboratory for observing changing phenocryst compositions and textures. J. Petrol. 46 (12), 2395–2426.
Tsuchiyama, A., 1985. Dissolution kinetics of plagioclase in the melt of the system diopside-albite-anorthite, and origin of dusty plagioclase in andesites. Contrib. Mineral. Petrol. 89 (1), 1–16.
Tsune, A., Toramaru, A., 2007. A simple model of oscillatory zoning in magmatic plagioclase: Development of an isothermal undercooling model. Am. Mineral. 92 (7), 1071–1079.
Turner, M.B., Cronin, S.J., Stewart, R.B., Bebbington, M., Smith, I.E.M., 2008. Using titanomagnetite textures to elucidate volcanic eruption histories. Geology 36 (1), 31–34.
Turner, M.B., Bebbington, M.S., Cronin, S.J., Stewart, R.B., 2009. Merging eruption datasets: Building an integrated Holocene eruptive record for Mt Taranaki, New Zealand. Bull. Volcanol. 71 (8), 903–918.
Turner, M.B., Cronin, S.J., Bebbington, M.S., Smith, I.E.M., Stewart, R.B., 2011. Integrating records of explosive and effusive activity from proximal and distal sequences: Mt. Taranaki, New Zealand. Quat. Int. 246 (1), 364–373.
Ubide, T., Kamber, B.S., 2018. Volcanic crystals as time capsules of eruption history. Nat. Commun. 9 article #326.
Ubide, T., McKenna, C.A., Chew, D.M., Kamber, B.S., 2015. High-resolution LA-ICP-MS trace element mapping of igneous minerals: In search of magma histories. Chem. Geol. 409, 157–168.
Ubide, T., et al., 2019a. Deep Magma Storage Revealed by Multi-Method Elemental Mapping of Clinopyroxene Megacrysts at Stromboli Volcano. Front. Earth Sci. 7.
Ubide, T., Mollo, S., Zhao, J.X., Nazzari, M., Scarlato, P., 2019b. Sector-zoned clinopyroxene as a recorder of magma history, eruption triggers, and ascent rates. Geochim. Cosmochim. Acta 251, 265–283.
Ubide, T., et al., 2023. Discrete magma injections drive the 2021 La Palma eruption. Sci. Adv. 9 (27), eadg4813.
Van Gerve, T., Neave, D., Almeev, R., Holtz, F., Namur, O., 2020. Zoned crystal records of transcrustal magma transport, storage and differentiation: insights from the Shatsky Rise oceanic plateau. J. Petrol. 61 (8), egaa080.
Vance, J.A., 1962. Zoning in igneous plagioclase: Normal and oscillatory zoning. Am. J. Sci. 260 (10), 746–760.
Viccaro, M., Giuffrida, M., Nicotra, E., Cristofolini, R., 2016. Timescales of magma storage and migration recorded by olivine crystals in basalts of the March–April 2010 eruption at Eyjafjallajökull volcano, Iceland. American Mineralogist 101 (1), 222–230.
Wager, L.R., Brown, G.M., Wadsworth, W.J., 1960. Types of igneous cumulates. J. Petrol. 1 (1), 73–85.
Waters, L.E., Lange, R.A., 2015. An updated calibration of the plagioclase-liquid hygrometer-thermometer applicable to basalts through rhyolites. Am. Mineral. 100 (10), 2172–2184.
Welsch, B., et al., 2016. Clinopyroxene in postshield Haleakala ankaramite: 2. Texture, compositional zoning and supersaturation in the magma. Contrib. Mineral. Petrol. 171 (1), 1–19.
Zellmer, G.F., 2021. Gaining acuity on crystal terminology in volcanic rocks. Bull. Volcanol. 83 (11), 78.
Zellmer, G.F., Annen, C., 2008. An introduction to magma dynamics. In: Annen, C., Zellmer, G.F. (Eds.), Dynamics of Crustal Magma Transfer, Storage and Differentiation. Geological Society, London, Special Publications, pp. 1–13.
Zellmer, G.F., Blake, S., Vance, D., Hawkesworth, C., Turner, S., 1999. Plagioclase residence times at two island arc volcanoes (Kameni Islands, Santorini, and Soufriere, St. Vincent) determined by Sr diffusion systematics. Contrib. Mineral. Petrol. 136 (4), 345–357.
Zellmer, G.F., Sparks, R.S.J., Hawkesworth, C.J., Wiedenbeck, M., 2003. Magma emplacement and remobilization timescales beneath Montserrat: insights from Sr and Ba zonation in plagioclase phenocrysts. J. Petrol. 44 (8), 1413–1431.
Zellmer, G.F., et al., 2016. Petrogenesis of antecryst-bearing arc basalts from the Trans-Mexican Volcanic Belt: Insights into along-Arc variations in magma-mush ponding depths, H2O contents, and surface heat flux. Am. Mineral. 101 (11), 2405–2422.
Zellmer, G.F., Iizuka, Y., Straub, S.M., 2024. Origin of crystals in mafic to intermediate magmas from circum-Pacific continental arcs: trancrustal magmatic systems versus transcrustal plutonic systems. J. Petrol. 65, egae013.
Zemeny, A., et al., 2023. Investigation of the Mid-Age (65–34 ka) Period of Taranaki Volcano, New Zealand: indications for the Effect of Volcano Growth. J. Petrol. 64 (5).
Zernack, A.V., Procter, J.N., 2021. Cyclic growth and destruction of volcanoes, Volcanic Debris Avalanches. Springer 311–355.
Zernack, A.V., Procter, J.N., Cronin, S.J., 2009. Sedimentary signatures of cyclic growth and destruction of stratovolcanoes: A case study from Mt. Taranaki, New Zealand. Sediment. Geol. 220 (3–4), 288–305.
Zernack, A.V., Cronin, S.J., Neall, V.E., Procter, J.N., 2011. A medial to distal volcaniclastic record of an andesite stratovolcano: Detailed stratigraphy of the ring-plain succession of south-west Taranaki, New Zealand. Int. J. Earth Sci. 100 (8), 1937–1966.